Identification of CD84 as a potent survival factor in acute myeloid leukemia

Yinghui Zhu[§*1-2-3], Mariam Murtadha[§2-3], Miaomiao Liu[§1], Enrico Caserta[2-3], Ottavio Napolitano[2-3], Le Xuan Truong Nguyen[3], Huafeng Wang[4], Milad Moloudizargari[2-3], Lokesh Nigam[2-3], Theophilus Tandoh[2-3], Xuemei Wang[1], Alex Pozhitkov[2-3], Rui Su[5], Xiangjie Lin[4], Marc Denisse Estepa[2-3], Raju Pillai[6], Joo Song[6], James F Sanchez[2], Yu-Hsuan Fu[3], Lianjung Zhang[3], Man Li[3], Bin Zhang[3], Ling Li[3], Ya-Huei Kuo[3], Steven Rosen[2], Guido Marcucci[3], John C. Williams[7], Flavia Pichiorri [*2-3]

[1]State Key Laboratory of Cardiovascular Diseases and Medical Innovation Center, Shanghai East Hospital, School of Life Sciences and Technology, Frontier Science Center for Stem Cell Research, Tongji University, Shanghai, 200092, China

[2]Judy and Bernard Briskin Center for Multiple Myeloma Research, Department of Hematology and Hematopoietic Cell Transplantation, City of Hope; Duarte, CA, USA.

[3]Department of Hematologic Malignancies Translational Science, Beckman Research Institute, City of Hope; Duarte, CA, USA.

[4]Department of Hematology, the First Affiliated Hospital, Zhejiang University School of Medicine, Zhejiang Provincial Key Laboratory of Hematopoietic Malignancy, Zhejiang University, Hangzhou, Zhejiang, 310000, PR China

[5]Department of System Biology, Beckman Research Institute, City of Hope; Duarte, CA, USA.

[6]Department of Pathology, City of Hope National Medical Center; Duarte, CA, USA.

[7]Department of Cancer Biology and Molecular Medicine, Beckman Research Institute, City of Hope; Duarte, CA, USA.

[§]These authors are co-first authors.

24 *Corresponding authors: Flavia Pichiorri, fpichiorri@coh.org;

25 City of Hope; 1500 E Duarte Rd, Duarte, CA, USA 91010.

26 Yinghui Zhu zhuyinghui@tongji.edu.cn

27 No. 1239, Siping Road, Yangpu District, Shanghai, 200092, China, Phone:+86-

28 021-65981041

29

30 Part of this work was presented in part at the American Society of Hematology Annual

31 Meeting in 2022 at New Orleans, LA.

32

Abstract

Acute myeloid leukemia (AML) is an aggressive and often deadly malignancy associated with proliferative immature myeloid blasts. Here, we identified CD84 as a critical survival regulator in AML. High levels of CD84 expression provided a survival advantage to leukemia cells, whereas CD84 downregulation disrupted their proliferation, clonogenicity and engraftment capabilities in both human cell lines and patient derived xenograft cells. Critically, loss of CD84 also markedly blocked leukemia engraftment and clonogenicity in *MLL-AF9* and *inv*(16) AML mouse models, highlighting its pivotal role as survival factor across species. Mechanistically, CD84 regulated leukemia cells' energy metabolism and mitochondrial dynamics. Depletion of CD84 altered mitochondrial ultra-structure and function of leukemia cells, and it caused down-modulation of both oxidative phosphorylation and fatty acid oxidation pathways. CD84 knockdown induced a block of Akt phosphorylation and down-modulation of nuclear factor erythroid 2-related factor 2 (NRF2), impairing AML antioxidant defense. Conversely, CD84 over-expression stabilized NRF2 and promoted its transcriptional activation, thereby supporting redox homeostasis and mitochondrial function in AML. Collectively, our findings indicated that AML cells depend on CD84 to support antioxidant pro-survival pathways, highlighting a therapeutic vulnerability of leukemia cells.

53 **Introduction**

54 Acute myeloid leukemia (AML) is a malignancy that rapidly progresses and presents with
55 uncontrollable accumulation of immature myeloid blasts in the bone marrow (BM) and
56 peripheral blood. Chemotherapy has been used to date as a standard treatment for AML
57 (1) and recently the development of novel therapeutic interventions, including the
58 introduction of the BCL2 inhibitor venetoclax, have positively impacted overall response
59 rates in AML, especially among younger patients (2). However, while the 5-year survival
60 rate for young patients is around 30%, for elderly patients it is as low as 5–10% (3),
61 indicating that further understanding of the disease biology is needed. Although AML is a
62 very heterogeneous disease characterized by cancer cell clones carrying different
63 molecular and cytogenetic abnormalities (4), it has been abundantly shown that
64 deregulation in the cellular redox networks associated with high reactive oxygen species
65 (ROS) levels are common features for AML cells (5). Several published data have shown
66 that an increase in redox state correlates with mutational events supporting oncogene
67 activation, tumor suppressor gene down-modulation, increased aerobic metabolism and
68 mitochondrial dysfunction (6). AML cells can survive high ROS levels by compensating
69 with molecular mechanisms that upregulate active antioxidant systems to avoid excessive
70 ROS accumulation and protect leukemic cells from oxidative stress-induced cell death (7,
71 8). Hence, down-regulation of the anti-oxidative pathways renders AML cells more
72 vulnerable compared to normal cells (9).

73 In AML cells, NRF2 (Nuclear factor E2-related factor 2) plays a pivotal role in regulating
74 oxidative stress pathways by transcriptionally activating antioxidant genes, essentially
75 protecting the cancer cells from damage caused by ROS and contributing to their

76 resistance to chemotherapy drugs (10, 11). Previously published data have shown that
77 NRF2 activation, protein stability and nuclear translocation strongly depends on the
78 phosphatidylinositol 3-kinase (PI3K)/AKT pathway, which is a survival pathway frequently
79 activated in AML patient blasts (12). When NRF2 translocate into the nucleus, it binds to
80 the antioxidant response element (ARE)-dependent cytoprotective genes (13). This
81 process leads to overexpression of several genes including antioxidant genes, anti-
82 apoptotic genes, and detoxifying genes (13), which contribute to cancer cell growth and
83 therapeutic resistance (12, 14, 15).

84 CD84 (SLAM5) is a member of the SLAM (signaling lymphocyte activation molecule)
85 family and is expressed at different levels in the normal hematopoietic lineage (16, 17).
86 Biochemical and structural studies indicate that CD84 forms homophilic dimers by self-
87 association (18), and in doing so, enhances interferon gamma (IFN-gamma) secretion
88 (19) and induces PD-L1 upregulation on chronic lymphocytic leukemia (CLL) cells,
89 resulting in suppression of T cell activation against cancer cells (20). Moreover, it has
90 been found that CD84 is an essential survival factor for CLL by activating a signaling
91 cascade that involves CD84 tyrosine phosphorylation, EAT-2 recruitment, and increased
92 AKT phosphorylation, resulting in BCL2 upregulation (21), a survival pathways that also
93 plays a pivotal role in AML pathophysiology (22). Recently, we (17) and others (17, 23)
94 have identified CD84 to be a robust myeloid derived suppressor cell (MDSCs) surface
95 marker, but its role in myeloid malignancies has yet to be investigated.

96 Here, we report that CD84 is a highly expressed tumor-associated target in AML. We also
97 report that CD84 suppression strongly limits AML cell growth and extends the survival of
98 AML xenografted mice. Finally, we observed that CD84 knockdown induces the

99 downregulation of antioxidant genes involved in glutathione metabolism through AKT
100 phosphorylation and NRF2 downmodulation. Our findings suggest that CD84 is a critical
101 survival factor regulating metabolic processes in leukemia cells, highlighting its role as a
102 potential therapeutic target for AML.

103

Results

CD84 is overexpressed in AML cells

To comprehensively characterize the expression pattern of CD84 in the hematopoietic system, we first examined its mRNA expression across various hematopoietic lineages using the BloodSpot database (GSE42519) (Figure S1A), and we also performed single-cell mass cytometry analysis of BM cells isolated from healthy donors (n=3) (Figure 1A, Table S1). The analysis revealed that CD84 is almost completely absent in normal hematopoietic stem cells (HSCs) and hematopoietic multipotent progenitors (MPPs). Conversely, CD84 levels are significantly upregulated in common myeloid progenitors (CMPs), granulocyte-monocyte progenitors (GMPs), early promyelocytes (early-PMs), and monocytes. Aligned with recently published data (24), significantly lower CD84 expression was observed in common lymphoid progenitors (CLPs) and the mature lymphoid lineage (Figure 1A and Figure S1A). These findings indicate that CD84 is predominantly expressed in early myeloid progenitors and their immediate derivatives, suggesting a potential role for CD84 in myeloid lineage early commitment. Because AML is characterized by the accumulation of clonal myeloid progenitors (25), we decided to investigate CD84 expression in this setting. Based on the gene expression profiling datasets that include large cohorts of patients with AML (GSE13159 and GSE9476), we observed that bone marrow mononuclear cells (BM-MNCs) of AML specimens showed statistically significant increase in *CD84* mRNA levels compared to those of normal healthy counterparts (Figure 1B-1C). By using the DepMap portal (https://depmap.org/portal/depmap/) (26), we analyzed *CD84* mRNA levels across the entire spectrum of human cancer cell lines (n=1197) and found a distinct elevated

127 expression of CD84 in leukemia, especially in AML cell lines (n=44), which we also
128 confirmed by flow cytometry analysis (n=9) (Figure S1B-1C). Consistently in AML cell
129 lines we found statistically significant correlation between mRNA and protein expression
130 (R=0.85, p=0.01, N=6) (Figure S1D). GEPIA (http://gepia.cancer-pku.cn) presented AML
131 as the predominant expresser of *CD84* (Figure S1E). Importantly, according to PRECOG
132 database analysis (http://precog.stanford.edu/) (27) and KMPlot database analysis
133 (https://kmplot.com/analysis/) (28), elevated *CD84* mRNA expression is associated with
134 shorter overall survival in patients with AML (GSE10358, *p*=0.01; KMPlot database,
135 *p*=0.028) (Figure S1F-1G) but this was not observed when The Cancer Genomic Atlas
136 (TCGA) and Beat AML genomic data sets were interrogated (29). We analyzed the
137 correlation between *CD84* expression and AML subtypes based on both molecular
138 classification, FAB subtypes or mutational status. In the GSE13159 database, the relative
139 expression of *CD84* over control was greater in karyotypes like inv(16), t(11q23)/MLL and
140 normal karyotype (p<0.0001), compared to t(15;17) and complex karyotype (p<0.05), but
141 absence of upregulation was found in t(8;21) (Figure S2A). AML subtypes with different
142 mutations show comparable expressions (Figure S2B-2C). FAB subtype analysis
143 revealed statistically significant lower *CD84* expression in M3 compared to other subtypes
144 (p<0.001), with comparable levels across non-M3 subtypes (Figure S2D). These findings
145 reinforce the relevance of CD84 in different AML subtypes. Flow cytometry analysis
146 confirms that CD84 is upregulated in primary AML samples obtained from different
147 sources (n=31) (Figure 1D), and AML cell lines (n=9) (Figure S1B), compared with levels
148 in healthy donor CD34+ cells (n=5) (Figure 1E-F), independent of disease status or
149 cytogenetic abnormalities (Table S2). Notably, high surface CD84 positivity (>70%) was

150 found in more than 50% of the AML samples, we analyzed (Table S3). Conversely to AML
151 cell lines, in primary AML samples obtained from different sources, we did not find direct
152 correlation between mRNA and protein expression (R^2=0.003, p=0.8, n=15), suggesting
153 that the heterogenicity of the primary sample population, which is different between
154 cohorts, may affect this analysis.

155 Aligned with this observation, a mass cytometry (CyTOF) panel was constructed to further
156 investigate CD84 expression across the cellular composition of AML samples (Table S1).
157 Using FlowSOM analysis, we observed CD84 to be predominantly within AML blast
158 populations, but that variable levels of non-cancer immune subsets were still detectable
159 in AML primary samples (Figure S2E). To further establish CD84 as a potential selective
160 target in leukemogenesis, we employed a tissue array assay to examine endogenous
161 expression of CD84 in normal tissue as well as AML BM. Immunohistochemistry (IHC)
162 analysis showed that, in normal tissue, CD84 positivity was exclusively detected in the
163 spleen, a major lymphoid organ (Figure 1G); this observation is in agreement with the
164 reported presence of variable expression of CD84 in the hematopoietic lineage (16), as
165 also confirmed by flow analysis in normal immune subsets isolated from healthy donors
166 (Figure S2F). Importantly, a strong CD84 signal was detected in almost 100% of the blasts
167 present in the BM biopsies obtained from patients with relapsing AML (n=15) carrying
168 different genetic abnormalities (Figure 1H; Figure S2G).

169 **CD84 downregulation impairs AML cell survival.**

170 To investigate the role of CD84 in AML, we conducted both gain- and loss-of-function
171 studies. We used the lentiviral vector-based shRNA system to knock down the expression
172 of CD84 (shCD84-1 and shCD84-2) (Figure 2A) and demonstrated that CD84

173 downregulation caused a statistically significant inhibition of cell growth (Figure 2B), as
174 well as induction of apoptosis in AML cell lines (Figure S3A-3B). While CD84 knockdown
175 did not affect the clonogenic activity of healthy donor derived CD34+ cell (Figure S3C), in
176 AML primary patient cells, we found that its downregulation substantially induced cell
177 apoptosis (Figure 2C; Figure S3D-3E) and inhibited cell colony formation (Figure 2D-2E).
178 To understand whether CD84 knockdown could also affect the ability of AML cells to
179 engraft, we downregulated CD84 in luciferase-expressing THP1 cells and transplanted
180 the cells into immunodeficient NSG mice. Attenuated tumor burden (Figure 2F) as well as
181 prolonged survival (Figure 2G) were observed in recipients of these cells, relative to the
182 control (p=0.0015). To further assess the importance of CD84 in regulating AML cell
183 engraftment capabilities, we ectopically over-expressed CD84 (CD84-OE) in THP1-
184 luciferase cells (Figure S3F-3G). Our in vivo data show that mice engrafted with THP-1
185 CD84-OE cells had a statistically significant reduction in survival, compared to control
186 group that was transduced with an empty-viral vector (mock) (Figure 2H-2I**,** p=0.002),
187 supporting that CD84 provided a further survival advantage in these cells. Notably, the
188 early mortality observed in the CD84-OE group was completely abolished when CD84
189 over-expression in THP-1 cells was knocked down by shRNA (CD84 OE+shCD84)
190 (Figure S3F-3G, Figure 2H-2I). At the time of relapse (~41 days) mice engrafted with
191 CD84 OE+shCD84 were euthanized to assess CD84 expression in the AML cells. Notably,
192 CD84 OE+shCD84 mice carried THP-1 cells that at relapse not only lost CD84 silencing
193 but maintained statistically significant CD84 upregulation compared to the mock/shCtrl
194 engrafted mice (p=0.045) (Figure 2J, Figure S3H), further supporting that CD84
195 overexpression facilitates AML progression, this effect being specifically mitigated by

196 CD84 deletion. To further investigate the role of CD84 in AML patient-derived cells, we
197 transplanted AML primary patient cells transduced with shCD84 or shCtrl plasmid into
198 NSG mice (Figure 3A; Figure S3I). We observed that AML burden was statistically
199 significantly lower in the BM (Figure 3B-3C; p=0.001, 51.2% vs 2.3%), spleen (Figure 3D;
200 p=0.026, 8.79% vs 0.84%) and PB (Figure 3E; p=0.035,13.06% vs 0.24%) in the CD84
201 knockdown group, compared with levels in the control recipient animals. We also found
202 reduced spleen weight in CD84 knockdown mice (Figure S3J-S3K) at the time the mice
203 were sacrificed (p=0.0416; 0.064g vs 0.032g). Moreover, we knocked down CD84 in a
204 luciferase-expressing AML PDX and transplanted them into immunodeficient NSG mice
205 (Figure S3L). Consistently, mice receiving CD84 knockdown cells exhibited reduced
206 tumor burden (Figure 3F) and extended survival (Figure 3G) compared to control animals.
207 We further validated in this experiment that the relapse observed in the shCD84 group
208 might be attributed to escape from shRNA knockdown (Figure S3M). To assess the
209 function of CD84 in AML cell maintenance, we employed a murine IL-3-dependent
210 myeloid cell line, 32D, for functional analysis, as endogenous CD84 is undetectable in
211 this line. We ectopically overexpressed wild type CD84 in 32D cells, or empty vector
212 (MOCK) as control. In the absence of murine IL-3, there was a more than 60% decrease
213 in apoptosis in CD84-expressing 32D cells induced by IL-3 deprivation, relative to MOCK
214 cells (p=0.0006) (Figure 3H-3I; Figure S3N). Our findings indicate that CD84 is required
215 for a distinct AML phenotype, including proliferation, clonogenicity and leukemic
216 engraftment.

217 **CD84 is essential for leukemia cell maintenance in AML mouse models.**

218 To understand the functional role of CD84 in leukemogenesis, we generated murine MLL-
219 AF9-HSPC pre-leukemic stem cells (LSCs) by transducing a hematopoietic stem cell-
220 enriched hematopoietic progenitor cell population (c-kit^{+}) with a lentivirus encoding the
221 *MLL-AF9* fusion oncogene (Figure 4A). We observed a statistically significant
222 upregulation of CD84 expression (Figure 4B; Figure S4A) and enhanced colony formation
223 (Figure S4B) in MLL-AF9 transduced c-kit+ cells compared to wildtype (WT) c-kit cells.
224 We knocked down mouse CD84 using two independent shRNAs (mouse shCD84-1 and
225 mouse shCD84-2) in MLL-AF9 cells and confirmed efficient knockdown at mRNA and
226 protein levels (Figure S4C-4E). As shown in Figure 4C, CD84 knockdown inhibited cell
227 growth. As expected, CD84 depletion dampened the clonogenic potential of MLL-AF9
228 AML cells (Figure 4D-4E) and induced apoptosis (Figure S4F). To evaluate the role of
229 CD84 in leukemogenesis *in vivo*, we conducted mouse BM transplantation assays in
230 irradiated C57BL/6 (CD45.1) syngeneic recipient mice (Figure 4A). We found that CD84
231 knockdown reduced leukemic engraftment in BM (Figure 4F-4G), spleen (SP) (Figure 4H)
232 and peripheral blood (PB) (Figure S4G), along with reduced splenomegaly (Figure 4I;
233 Figure S4H), compared with levels in recipients without CD84 silencing. Notably, CD84
234 knockdown also reduced the immature blast cell population (Figure 4J). In secondary BM
235 transplantation, leukemic engraftment was further attenuated in the CD84 knockdown
236 group, resulting in a statistically significant increase in the median survival (66 days)
237 compared to that of the control group animals (median survival 48 days; p=0.0016)
238 (Figure 4K-4M). Because our data have shown that AML cells transduced only with one
239 CD84 silencing sequence can overcome shCD84 *in vivo*, to enhance the efficiency of
240 CD84 knockdown, and to conduct longer term *in vivo* studies, we transfected MLL-AF9

241 cells with both shCD84-1 and shCD84-2 targeting CD84. CD84 expression was
242 abrogated when AML cells were treated with the double CD84 knockdown (Figure S4I).
243 Correspondingly, the colony formation assay revealed a complete absence of colony
244 formation in the CD84 knockdown group (Figure S4J-4K). In addition, we employed a
245 second mouse AML model harboring inv(16) (p13q22), which creates the fusion gene
246 *CBFB-MYH11* (CM). We transduced CD84 shRNA and control shRNA into leukemic BM
247 cells collected from primary AML mice bearing CM/inv (16) AML (30). Consistent with the
248 observations in MLL-AF9 AML studies, CD84 was upregulated in inv(16) leukemic (c-kit+)
249 cells (Figure 5A). CD84 knockdown substantially arrested inv(16) AML cell growth and
250 increased apoptosis (Figure S4L; Figure 5B-5C). CD84 deficiency also disrupted the
251 leukemogenic potential of inv (16) AML cells, decreasing by more than 80% the leukemic
252 engraftment in the BM ($p<0.0001$), spleen ($p=0.004$) and PB ($p=0.014$) of recipients
253 (Figure 5D-5E; Figure S4M), leading to a substantial reduction in spleen weight (Figure
254 S4N-4O), compared to mice carrying leukemia cells with intact CD84 expression.
255 Consistently, when we transfected inv(16) AML cells with both shCD84-1 and shCD84-2
256 to target CD84 no colonies were formed in the CD84 knockdown group (Figure 5F-5G;
257 Figure S4P). Collectively, these data demonstrate that CD84 plays a critical role for AML
258 maintenance *in vivo* and its role as survival factor in AML cells is conserved across
259 models.

260 **CD84 knockdown deactivated energy metabolism and induced mitochondrial**
261 **stress in AML**

262 To further elucidate the molecular underpinnings of CD84 in leukemia cells, we induced
263 alterations in the expression of endogenous CD84 and performed RNA-seq. Specifically,

264 we transfected with shCtrl or shCD84 lentivirus (Figure 6A-6B) two AML cell lines (HEL
265 and THP-1) that maintain high CD84 expression. Gene set enrichment analysis (GSEA)
266 showed that CD84 knockdown in both lines caused downregulation of gene sets involved
267 in energy metabolic pathways (Figure S5A-5B), including fatty acid metabolism, glycolysis,
268 and oxidative phosphorylation, especially in HEL cells. As further emphasis of the
269 common signature associated with CD84 downmodulation, all differentially expressed
270 genes (DEGs) identified in the shCD84 versus shCtrl groups in the two cell lines, and 188
271 common genes were found (Figure 6C-6D). Gene Ontology enrichment analysis indicated
272 that small molecule metabolic pathways including amino acid metabolism and lipid
273 metabolic processes were downregulated upon CD84 knockdown (Figure 6E, Figure
274 S5C).

275 Altogether, these results demonstrate that CD84 may orchestrate AML cell survival
276 through modulating energy metabolic reprogramming. To define the role of CD84 in
277 regulating mitochondrial function, we examined alteration of mitochondrial fitness
278 including oxygen consumption rate (OCR), extracellular acidification rate (ECAR), fatty
279 acid oxidation (FAO), mitochondrial morphology, mitochondrial membrane potential and
280 mitochondrial biogenesis upon CD84 deletion. CD84 depletion caused mitochondrial
281 dysfunction as indicated by decreasing OCR and ECAR (Figure 6F) and FAO (Figure 6G)
282 in an AML cell line. Importantly, we also validated the attenuated OCR and ECAR in three
283 AML primary cells following CD84 downregulation (Figure 6H). Next, we investigated the
284 effects of CD84 deletion on mitochondrial dynamics in AML cells. Accordingly, we found
285 that CD84 deletion caused disruption of mitochondrial matrix morphology and loss of
286 mitochondrial cristae (Figure 7A). Moreover, CD84 knockdown substantially attenuated

287 TOM20 (mitochondrial marker), MFN1 (mitochondrial fusion marker) and HMGB1
288 expression levels, which indicated mitochondrial dysfunction upon CD84 deletion in AML
289 (Figure 7B). Additionally, mitochondrial membrane potential (MMP) is an indicator of
290 mitochondrial function, and loss of MMP often suggests mitochondrial dysfunction (31).
291 Flow cytometry analysis of JC-1 staining demonstrated a substantially decreased
292 intensity of aggregates and increased intensity of monomers, indicating a substantial loss
293 in MMP and resultant mitochondrial dysfunction in CD84-deleted cells (Figure 7C; Figure
294 S5D). Importantly, the reintroduction of CD84 expression partially rescued mitochondrial
295 dysfunction as indicated by mitochondrial membrane potential (Figure 7D-7E). CD84
296 over-expression also rescued MFN1 protein downregulation and as previously published
297 (20) phosphorylation of AKT (p-AKT) (Figure 7F). Collectively, these investigations
298 present compelling evidence that CD84 plays a pivotal role in regulating the survival of
299 AML through orchestrating energy metabolism and inducing mitochondrial stress.

300 **CD84 knockdown impairs glutathione metabolism and NRF2 antioxidant defense,**
301 **leading to mitochondrial dysfunction in AML**

302 To further investigate the underlying mechanism associated with mitochondrial
303 dysfunction induced by CD84 deletion, we further performed KEGG pathway analysis and
304 observed that the glutathione (GSH) metabolism pathway was highly enriched upon
305 CD84 knockdown (Figure 8A). We found and further validated that almost all the genes
306 involved in the GSH metabolism were consistently downregulated upon CD84 knockdown,
307 including key genes involved in GSH synthesis, such as glutamate-cysteine ligase
308 catalytic subunit (GCLC) and glutamate-cysteine ligase modifier subunit (GCLM), among
309 others (Figure 8B-8C). Consistently, the protein expression of GCLM and GCLC were

310 robustly decreased in CD84 knockdown cells (Figure 8D). In cancer cells, a high level of
311 GSH is indispensable to scavenge excessive ROS and detoxify xenobiotics, which make
312 it a potential target for cancer therapy (32, 33). Our results exhibited that CD84
313 knockdown resulted in enhanced ROS generation (Figure 8E-8F) and reduced levels of
314 GSH (Figure 8G) in AML cells. These results are aligned with the well-known concept
315 that GSH downregulation is associated with impairment of the electron transport chain
316 (ETC) in mitochondria (34). Because GSH metabolism genes including GCLC and GCLM
317 are downstream targets of NRF2 (35) and CD84 pro-survival activity has been linked to
318 SHIP-1-AKT phosphorylation (21), which in turn has been associated to Nrf2
319 transcriptional activation (36-39), we investigated whether changes in CD84 expression
320 may affect NRF2 activity. We observed that CD84 knockdown in AML cells decreased
321 total NRF2 protein levels (Figure S6A) and its nuclear localization (Figure 8H-8I).

322 The decreased expression and nuclear distribution of NRF2 induced by knockdown of
323 CD84 were rescued by stably overexpressing CD84 (Figure 9A), suggesting that CD84
324 is critical for maintaining the nuclear translocation of NRF2. NRF2 is a transcription factor
325 that coordinates the basal and stress-inducible activation of a vast array of cytoprotective
326 genes through antioxidant response elements (AREs). To fully assess the functional
327 status of the NRF2-ARE pathway, we measured its transcriptional activity using ARE-
328 driven luciferase constructs. We observed that stable over-expression of CD84 activated
329 ARE-regulated luciferase in HEK 293T cells compared to cells transduced with empty
330 vector (EV), and the elevated activity was statistically significantly reduced subsequently
331 by CD84 knockdown (Figure S6B-S6C). Because NRF2 protein stability and nuclear
332 translocation is tightly regulated by mechanisms of ubiquitination (40), we investigated

333 whether CD84 knockdown could promote NRF2 ubiquitination and subsequent
334 degradation. Immunoprecipitation assays show a concomitant decrease in NRF2 but an
335 increase in its ubiquitination upon shCD84 (Figure 9B and Figure S6D). Western blot
336 analysis showed that the treatment of the protein synthesis inhibitor CHX further
337 decreased protein level of NRF2 in shCD84 group, based on elevated proteolytic
338 degradation (Figure 9C; Figure S6E). Because nucleoplasm distribution and protein
339 stability of NRF2 is an important regulatory event that is tightly controlled by its association
340 with a cytosolic inhibitor protein, KEAP1 (41), a sensor protein that targets NRF2 for
341 ubiquitination by a Cullin-3-dependent mechanism and leads to proteosome-dependent
342 degradation (42), we investigated KEAP1 binding to NRF2 upon CD84 modulation.
343 Immunoprecipitation data show that upon CD84 knockdown there is an increase in NRF2-
344 KEAP1 binding associated with NRF2 protein downregulation (Figure 9D, Figure S6F),
345 an effect that was reverted upon CD84 over-expression (Figure 9E, Figure S6G). These
346 findings provided a novel mechanism in that CD84 is involved in maintaining NRF2
347 transcription activity and the mitochondrial antioxidant system in AML.

348

349 **Discussion**

350 CD84 is an hematopoietic marker that is variably expressed on distinct subsets of B and
351 T cells, but it is also observed to be consistently expressed at high levels on monocytes,
352 macrophages, dendritic cells, platelets and MDSCs (23, 43). We show that CD84 is a
353 hematopoietic lineage marker and its expression in absent in normal tissues. Here we
354 show that normal HSCs and MPPs are also negative for CD84 and, that during the
355 hematopoietic differentiation process, CD84 begins to be expressed at high levels in
356 CMPs. Although AML is characterized by the accumulation of CMPs, the role of CD84 in
357 this disease setting has not been investigated thus far. Previously published data have
358 shown that CD84 positively regulates LPS-induced cytokine secretion through MAPK
359 phosphorylation and NF-kB activation in macrophages (43), two survival pathways that
360 are critical to support AML progression and drug resistance (44-49). Consistent with
361 previously published data showing the pivotal role of CD84 in supporting CLL cell survival
362 and growth (20, 21), our data suggest that CD84-dependent survival effects appear to be
363 even more prominent in AML. Gene disruption via short hairpin RNA in AML lines, AML
364 primary patient cells and murine models showed that CD84 depletion robustly hampered
365 AML cell survival, blast clonogenicity and leukemic engraftment. In support that CD84
366 expression confers strong survival advantages to AML cells, we observed that mice
367 xenografted with CD84 over-expressing cells had statistically significant lower survival
368 compared control animals, an effect that was completely reverted by CD84 knockdown in
369 the same experimental setting. Although a delay of symptomatic disease was observed
370 in AML xenograft models transplanted with either AML cell lines or patient derived
371 xenograft carrying shCD84 knockdown, at the time of relapse AML cells completely

372 bypassed CD84 silencing, further supporting the clonal advantage associated with the
373 expression of high CD84 levels in leukemia cells.

374 We found direct correlation between CD84 mRNA expression and survival of AML
375 patients in two out of four mRNA sequencing data sets. Interestingly, conversely to AML
376 cell lines, we did not find direct correlation between CD84 surface expression and mRNA
377 in primary AML samples obtained from different sources. These data may suggest that
378 AML cell heterogenicity both in terms of genetic and cellular composition, and blast cell
379 purity may be responsible. This concept is also supported from our immune
380 histochemistry analysis (IHC) in which we found in all the AML samples analyzed almost
381 100% of the blasts are highly positive for CD84, but this positivity was somehow diluted
382 when the samples were analyzed by both flow cytometry and CyTOF. We acknowledge
383 that our IHC analysis is based on a limited number of samples and needs further
384 investigation.

385 Consistent with these observations, shRNA targeting CD84 in two pre-leukemic AML
386 mouse cells, MLL-AF9 and inv(16) AML, inhibited cell viability and delayed leukemic
387 onset in recipient mice. Notably, in both immune competent AML mouse models CD84
388 up-regulation was observed only in leukemic c-kit+ but not in the healthy counterpart.
389 With the intent to generate stable AML clones that maintained CD84 downregulation, our
390 data show that, when CD84 was completely downmodulated using a double shCD84
391 targeting, mouse leukemia cells lost their clonogenic capabilities, resulting in a complete
392 absence of colonies, further supporting that CD84 upregulation is essential for the
393 leukemogenesis process, and its role is conserved through the species.

394 Recently, therapeutically targeting the metabolic vulnerability of leukemia cells through
395 mitochondrial alterations has attracted much interest in the AML community (50, 51). This
396 interest is based on the dependence of AML cells on oxidative phosphorylation (52, 53),
397 fatty acid metabolism (54), their ability to tolerate higher ROS levels (9, 55, 56), and their
398 low tolerance to the downregulation of anti-oxidant enzymes (9). In agreement with these
399 data, GSEA enrichment analysis revealed that CD84 downregulation in AML cells affects
400 metabolic processes involving mitochondria function. In fact, it is reported that AML
401 progression requires increased mitochondrial biogenesis and oxidative phosphorylation
402 (53) and that the quiescent leukemic stem cells are more dependent on oxidative
403 phosphorylation, as they cannot efficiently utilize glycolysis for energy homeostasis (57,
404 58). In CLL, CD84 is reported as a positive regulator of anti-apoptotic genes, such as
405 BCL2 and MCL1 (21), which is also associated with mechanisms of tolerance to oxidative
406 stress (59). GSEA enrichment analysis revealed that CD84 downregulation in AML cells
407 substantially affects metabolic processes involving mitochondrial function such as fatty
408 acid metabolism and oxidative phosphorylation. CD84 knockdown downregulates AKT
409 phosphorylation, alters the structure of mitochondria, disrupts mitochondrial respiration,
410 and decreases oxidative phosphorylation. These observations suggest that impairing
411 CD84 activation pathways could be therapeutically beneficial in the treatment of patients
412 with AML. In mechanism study, we observed that CD84 appears to play a pivotal role in
413 maintaining glutathione metabolism and NRF2 antioxidant defense in leukemia cells
414 causing ROS accumulation. Knockdown of CD84 decreases NRF2 nuclear localization
415 and transcriptional activity of anti-oxidant genes increases oxidative stress, and promotes
416 NRF2 degradation via the KEAP1 interaction. Although further studies are needed to

417 identify further key components and specifically characterize the cascade of events by
418 which CD84 can regulate NRF2 degradation, to the best of our knowledge we show for
419 the first time that CD84 plays an essential role in regulating AML metabolisms and
420 oxidative phosphorylation, highlighting a dependency of AML to CD84 expression.
421 Notably, we (17) and others (17, 23) have recently identified CD84 to be highly expressed
422 in MDSCs. Interestingly MDSCs can produce high levels of ROS to fulfill their immune
423 suppressive activity, but their viability remains unaffected mainly through NRF2-driven
424 antioxidant capacity (60-62). Although the biological function of CD84 on the surface of
425 MDSCs has not been yet elucidated, we can speculate that, in this heterogeneous
426 myeloid cell population as well, CD84 may be crucial in empowering an antioxidant
427 defense to preserve cellular viability, an observation that needs further research.

428 In conclusion, we show that CD84 is required for AML cell survival and leukemogenesis.
429 Mechanistically, we reveal that CD84 regulates AML survival through modulating NRF2
430 transcriptional activity involved in the mitochondrial antioxidant system. Finally, we
431 identify CD84 as critical regulator of mitochondrial oxidative stress, highlighting a
432 therapeutic vulnerability of AML cells.

433

434 **Methods**

435 ***Sex as a biological variable.*** Our study examined male and female animals, and similar
436 findings are reported for both sexes.

437 ***Cell culture.*** AML primary patient cells were cultured in Stemspan serum-free medium
438 (StemCell Technologies), supplemented with low concentrations of growth factors (GFs)
439 similar to those present in long-term BM stromal cell culture (200 pg/mL granulocyte-
440 macrophage colony-stimulating factor [GM-CSF], 50 pg/mL leukemia inhibitory factor
441 [LIF], 1 ng/mL granulocyte colony-stimulating factor [G-CSF], 200 pg/mL stem cell factor
442 [SCF], 200 pg/mL macrophage inflammatory protein-1α [MIP-1α], and 1 ng/mL
443 interleukin-6 [IL-6]). The THP1, SKM1, HEL (HEL 92.1.7), NOMO1, U937, (kindly
444 provided by Dr. Ling Li laboratory at City of Hope) and MV-4-11 (purchased from ATCC,
445 CRL-9591) cell lines and the multiple myeloma cell line MM1S were maintained in
446 RPMI1640 with 10% FBS, penicillin, streptomycin and glutamine (all Gibco-BRL). The
447 HEK-293T line was maintained in DMEM with 10% FBS, penicillin, streptomycin and
448 glutamine (all Gibco-BRL). MLL-AF9 AML cells were cultured in IMDM with 10% FBS,
449 penicillin, streptomycin and glutamine (all Gibco-BRL) supplemented with 2 ng/mL IL-3.
450 *Inv* (16) AML cells were cultured in IMDM with 20% FBS, penicillin, streptomycin and
451 glutamine (all Gibco-BRL) supplemented with 20 ng/ml SCF, 20 ng/ml TPO, 10 ng/mL IL-
452 3 and 6 ng/ml IL-6. Cells were grown at 37°C in an atmosphere containing 5% CO_2.

453 ***Lentivirus transduction of cell lines*** Lentivirus pseudotyped particles were produced
454 by Lipofectamine 2000 (Life Technologies) –mediated transfection of 293T cells with the
455 packaging construct psPAX2, a plasmid carrying G-glycoprotein of vesicular stomatitis
456 virus (VSV-G), and the lentivirus vectors including MSCV-Luciferase-EF1α-copGFP-T2A-

457 Puro (System biosciences, SBI), pMIG-FLAG-MLL-AF9 (addgene), pCDH-EF1α-MCS-
458 T2A-GFP (addgene), pCDH-EF1α-MCS-T2A-GFP-CD84 (genescript), PLKO.1-puro-
459 shCD84-1(TRCN0000057474; CGCTACAACCTGCAAATCTAT; human; Millpore Sigma),
460 PLKO.1-puro-shCD84-2 (TRCN0000371708; TTATGGCACACTGGGATAAAC ; human;
461 Millpore Sigma), PLKO.1-puro-shCD84-1 (TRCN0000066279;
462 GCAGACATCAATGAAGAGAAT ; mouse; Millpore Sigma), and PLKO.1-puro-shCD84-1
463 (TRCN0000066280; GCAGATGATGTCTCAAAGAAA; mouse; Millpore Sigma). Viral
464 supernatants were harvested at 48 and 72 hours after transfection and filtered through a
465 0.45 mm low protein binding membrane (Millipore). Cells were exposed to virus-
466 containing supernatant (MOI=5-10) via spinoculation and then sorted by flow cytometry
467 based on GFP or selected by puromycin selection (1 µg/ml).

468 ***MLL-AF9 retrovirus packaging*** HEK293T cells were plated overnight in T75 flask at a
469 density of 8 millions cells per flask. Next day, cells were transfected with 10 µg of pMIG-
470 FLAG-MLL-AF9 (addgene, catalog # 71443) and 7 µg of pCL-ECO plasmids using
471 Lipofectamine 3000 transfection reagent for eight hours in Opti-MEMTM medium
472 (ThermoFisher, catalog # 31985062). At eight hours post transfection, Opti-MEM medium
473 was replaced with complete DMEM medium. Viral containing supernatant was collected
474 at 48 and 72 hours and concentrated with Retro-Concentin (SBI, catalog # RV100A-1) for
475 72 hours at 4°C and virus pellet was resuspended in 1X DPBS and frozen.

476 ***Transduction of c-Kit^{+} cells with MLL-AF9 retrovirus*** C57BL/6 mice were humanely
477 euthanized, and femurs, tibias, and spine were harvested and crushed to collect the
478 mononuclear cells (MNCs). Following manufacturer's protocol (Miltenyi Biotec, catalog #
479 130-091-224), c-Kit positive cells were isolated from MNCs and transduced with MLL-

480 AF9 retrovirus as described previously with modifications (63). Briefly, non-treated 24 well
481 plate was coated with 20 µg/ml Retronectin (Takara, catalog # T100A) overnight at 4°C.
482 Following overnight incubation, Retronectin was washed, and plate was blocked with 2%
483 BSA/1XDPBS for 30 minutes at room temperature and MLL-AF9 retrovirus was
484 spinoculated for 2 hours at 1000 x g/4°C. The spinoculation with viral supernatant was
485 repeated at least three times. Following spinoculation, viral supernatant was aspirated
486 and c-Kit+ cells were added to the plate and repeated spinoculation for 10 minutes at
487 room temperature. At 24 hours, MLL-AF9-c-Kit+ transduced cells were recollected and
488 added to new non-treated 24-well plate that was coated with Retronectin and
489 spinoculated twice with MLL-AF9 retrovirus. c-Kit+ cells were resuspended in 20% FBS/1%
490 penicillin-streptomycin IMDM medium with following cytokines: 20 ng/ml murine IL-3
491 (GeminiBio, catalog # 300-324P-100), 20 ng/ml murine IL-6 (Invitrogen, catalog # RMIL6I),
492 and 60 ng/ml murine stem cell factor (SCF) (Invitrogen, catalog # RP-8632) and 10 µg/ml
493 of polybrene. At 48 hours, MLL-AF9 GFP+ c-Kit+ cells were transduced with shCtrl and
494 shCD84 lentivirus for 48 hours at MOI=5. At 48 hours post shCtrl and shCD84
495 transduction, cells were collected for apoptosis analysis and colony forming assay.

496 ***Flow cytometry analysis*** Cells were washed with 1X PBS and stained for 30 minutes in
497 ice-cold FACS buffer (PBS+2%FBS) using antibodies (anti-human CD84-PE, Biolegend,
498 catalog # 326008; anti-human CD45-APC, Biolegend, catalog # 368512; anti-human
499 CD33-FITC, eBioscience; anti-mouse CD45.1, Biolegend; anti-mouse CD45.2, BD,
500 catalog # 565390; anti-mouse CD84-PE, Biolegend, catalog # 122806). After 30 min, cells
501 were washed and analyzed on LSRII (Becton Dickinson) or BD LSR Fortessa X-20
502 (Becton Dickinson). Analysis was conducted using FlowJo™ Software (version 10.7.1).

503 The stained samples were analyzed on BD LSR Fortessa X-20 (Becton Dickinson).
504 Analysis was conducted using FlowJo™ Software (version 10.7.1).

505 ***Analysis of cell viability, apoptosis, and colony formation assay*** Cell growth was
506 measured utilizing the CellTiter-Glo® Luminescent Cell Viability Assay Kit (Promega).
507 Cell proliferation was determined using dye eFluor 670 staining (eBioscience) followed
508 by flow cytometry analysis. Apoptosis was assessed based on Annexin V/DAPI staining
509 (eBioscience). For colony-forming assay, cells were resuspended in 2% IMDM at
510 concentration of 0.1 million cells/ml, and 100 µl of this suspension was added to one well
511 of 24 well plate and each treatment was plated in at least duplicates and repeated at least
512 three times. Human cells were overlaid with 750 µl of MethoCult™ H4034 (Stem Cell
513 Technologies) and murine cells were overlaid with 750 µl of MethoCult™ GF M3434
514 (Stem Cell Technologies, catalog # 03444). Colonies were analyzed on day 14 using
515 Widefield Zeiss Observer 7 inverted microscope in tiles at City of Hope Light Microscopy
516 Imaging Core.

517 ***Seahorse Assay*** A total of 40,000 cells in 200 µL cell culture medium was seeded in
518 each well of an XF-96-well cell culture microplate (Seahorse Bioscience) and cultured
519 overnight at 37°C in 5% CO_2. As a negative control, three wells were kept devoid of cells
520 and given only Seahorse media, which comprises basal XF media, 5.5 mM glucose,
521 1 mM sodium pyruvate and 4 mM glutamine. (Additionally, the pH was adjusted to 7.4.)
522 Twelve hours prior to running a plate, the Seahorse sensor cartridge was incubated with
523 Seahorse Calibrant solution according to the manufacturer's protocol, in a 37°C, CO_2-free
524 incubator. On the day of an assay, shCtrl and shCD84 cells were washed and incubated
525 with Seahorse media. The sensor cartridge was fitted onto the cell culture plate, which

526 was then placed into a 37 C, CO_2-free incubator for 1 h. During the assay, which was run
527 on the Seahorse XF96 Analyzer, the following inhibitors were injected sequentially, as is
528 standard for the Cell Energy Test: oligomycin (1 mM), FCCP (0.5 mM).

529 ***Reactive Oxygen Species and Glutathione Measurement*** THP1 and HEL cells
530 transfected with shCtrl or shCD84 were washed with 1X PBS and then incubated with
531 5μM CellROX® Oxidative Stress Reagents (Invitrogen, USA, Cat#C10422) for 30min at
532 37°C in the dark. After incubation, cells were washed twice with 1X PBS and analyzed on
533 CytoFLEX LX flow cytometer (Beckman Coulter). Data were analyzed using FlowJo™
534 Software (version 10.7.1). For glutathione (GSH) measurement, the levels of GSH were
535 assessed using a commercially available kit (Beyotime, China, Cat# S0053) according to
536 the manufacturer's instructions. Briefly, cell samples were subjected to two rapid freeze–
537 thaw cycles using liquid nitrogen and a 37 °C water bath. Corresponding detection
538 reagents were added to an appropriate volume of cell lysates. After incubation for 25 min,
539 GSH content was measured using a microplate reader at an absorbance of 412 nm. GSH
540 levels were quantified by comparing the absorbance values to a standard curve.

541 ***Immunofluorescence staining*** The cultured cells were fixed in 4% paraformaldehyde
542 (PFA) for 25 min in dark at room temperature (RT). After fixation, cells were permeabilized
543 and blocked with 3% donkey serum in PBS containing 0.2% Triton X-100 for 60 min at
544 RT. After centrifugation at 1,000×g for 5 min, cells were incubated with primary antibodies
545 (NFE2L2 Polyclonal antibody, Proteintech, China, Cat#16396-1-AP) overnight at 4 °C.
546 The next day, cells were incubated with the appropriate secondary fluorescently labeled
547 antibodies (CoraLite594-conjugated Goat Anti-Rabbit IgG(H+L), Proteintech, China,
548 Cat#SA00013-4) for 1 hour in dark at RT. After incubation, the samples were mounted

549 using ProLong™ Gold Antifade Mountant with DAPI (Invitrogen, USA, Cat#P36941).
550 Imaging was performed using a laser scanning confocal microscope (OLYMPUS,
551 FV3000).

552 ***Morphological analysis*** In brief, cells were extracted from BM and diluted in PBS to
553 $2x10^5$/ml. After they were spread onto slides, cells were fixed in absolute methanol and
554 stained in Wright-Giemsa Stain Solution (Sigma). Smears were then rinsed in pH 6.6
555 phosphate buffer solution. Images were acquired using Zeiss Observer 7.

556 ***RNA-seq analysis*** THP1 and HEL cells with shCtrl or shCD84 were selected by
557 puromycin selection. Cells were collected and resuspended in Trizol reagent (Invitrogen
558 Corporation) following the manufacturer's instructions. RNA quality (RNA integrity
559 number [RIN]) was assessed using an Agilent Bioanalyzer, and all samples were
560 evaluated as RIN > 8. RNA sequencing libraries were prepared with Kapa RNA
561 HyperPrep kit with polyA kit (Kapa Biosystems, Cat KR1352) according to the
562 manufacturer's protocol. Sequencing run was performed in the single read mode using
563 Illumina HiSeq 2500. Sequenced reads were aligned to the mouse hg38 reference
564 genome with TopHat2 (v 2.0.14). Gene expression level was quantified using HTSeq (v
565 0.6.1), and differential expression analysis was performed using DESeq2 (v 1.14.1).

566 ***Mass cytometry (CyTOF) staining and acquisition*** BM or PB MNCs from AML patients
567 were thawed in customized thawing medium (20% FBS, 0.06 mg/ml DNAse I, and 20,000
568 U heparin in IMDM) for 2 hours at room temperature to obtain single cells. Following 2
569 hours of incubation, AML MNCs were washed and suspended in IMDM supplemented
570 with 20% FBS. A total of $2\text{-}4x10^6$ BM MNCs were stained with a custom panel of 39 metal-
571 conjugated antibodies for surface markers along with Cell-ID cisplatin for non-viable cell

572 detection (see Table S1). Staining protocols provided by Standard BioTools Inc. were
573 followed for Cell-ID Cisplatin (PRD018 version 5) (Cat. 201064) and Maxpar
574 Cytoplasmic/Secreted Antigen Staining with Fresh Fix (400279 Rev 05). Purified
575 antibodies were purchased from BioLegend and conjugated in-house using Maxpar
576 Antibody Labeling (PRD002 Rev 12) from Standard BioTools. Stained samples were
577 acquired on a Helios mass cytometer (Standard BioTools).

578 ***CyTOF data cleanup and analysis*** Data from the Helios mass cytometer was bead
579 normalized per manufacturer's recommendations using standalone CyTOF Software
580 7.0.8493.0. For analysis, the FCS files obtained from the custom panel were manually
581 analyzed using two software platforms. FlowJo™ Software (Windows edition, Version
582 10.6, Becton Dickinson Company; 2019) was utilized for overall cleaning before exporting
583 to the Cytobank platform. The Cytobank© platform (Cytobank, Inc., Mountain View, CA)
584 accessible at https://www.cytobank.org was employed for further analysis of gating, tSNE
585 plots, and FlowSOM analysis for AML subset populations.

586 ***Immunohistochemistry (IHC)*** CD84 IHC was performed on Ventana Discovery Ultra
587 IHC automated stainer (Ventana Medical Systems, Roche Diagnostics, Indianapolis,
588 USA). Briefly, the tissue slides were deparaffinized, rehydrated and incubated with
589 endogenous peroxydase activity inhibitor and antigen retrieval solution. Then, the anti-
590 CD84 primary antibody (Abcam, catalog # ab131256) was incubated followed
591 by DISCOVERY anti-Rabbit HQ and DISCOVERY anti-HQ-HRP incubation. The stains
592 were visualized with DISCOVERY ChromoMap DAB Kit, counterstained with
593 haematoxylin (Ventana) and coverslipped. IHC whole slide images were acquired with

594 NanoZoomer S360 Digital Slide Scanner (Hamamatsu) and viewed by NDP.view image
595 viewer software.

596 ***Nuclear and cytoplasmic protein extraction*** The nuclear and cytoplasmic proteins
597 were obtained using the Nuclear and Cytoplasmic Protein Extraction Kit (Beyotime, China,
598 P0027) following the manufacturer's instructions. Cytoplasmic Protein Extraction: Cells
599 were collected and resuspended in 100–200 μL of Cytoplasmic Extraction Buffer,
600 supplemented with protease and phosphatase inhibitors. The lysate was incubated on ice
601 for 10 minutes, vortexed, and centrifuged at 12,000×g for 10 minutes at 4°C. The
602 supernatant (cytoplasmic fraction) was collected and stored. Nuclear Protein Extraction:
603 The pellet was resuspended in 50–100 μL of Nuclear Extraction Buffer and incubated on
604 ice for 30 minutes with vortexing. After centrifugation Protein concentrations were
605 determined using a BCA protein assay kit (Thermo Fisher Scientific, Cat# 23225).

606 ***Coimmunoprecipitation assay*** THP1 or HEL cells transduced with shCtrl or shCD84
607 were collected and lysed in NP-40 lysis buffer (0.5M EDTA, 1% NP-40) supplemented
608 with protease inhibitors. The lysates were incubated on ice for 30 min and sonicated (10
609 brusts of 5 seconds on,5 seconds off) and centrifuged at 12,000×g for 15 min at 4 °C.
610 Protein concentrations were determined using a BCA protein assay kit (Solarbio, China,
611 Cat#PC0020). A small aliquot of lysate was saved as input. The remaining supernatant
612 was incubated with the primary antibody (NRF2 Polyclonal antibody, Proteintech, China,
613 Cat#16396-1-AP; KEAP1 Monoclonal antibody, Proteintech, China, Cat#60027-1-Ig;
614 DYKDDDDK tag Monoclonal antibody (Binds to FLAG® tag epitope), Proteintech, China,
615 Cat#66008-4-Ig) or normal IgG (rabbit: CST, USA, Cat#2729S; mouse: SCBT, USA,
616 Cat#sc-2025) overnight at 4 °C. Following incubation, the lysate was further incubated

617 with precleaning protein A/G beads (MCE, USA, Cat#HY-K0202) for 4 hours at 4°C. After
618 three washes with washing buffer (0.5M EDTA, 0.1% NP-40), the beads were
619 resuspended in 60 μl of 1× loading buffer, boiled and then subjected to SDS–PAGE for
620 further analysis.

621 ***Western blotting analysis*** Briefly, equal amounts of extracts were loaded onto the SDS
622 polyacrylamide gels, electrophoresed, and blotted onto the PVDF membranes (Millipore,
623 USA, Cat#IPVH00010). The membrane was blocked with 5% skimmed milk, followed by
624 incubation with primary antibodies at 4 °C overnight. Then, the membranes were
625 incubated with the HRP-conjugated secondary antibodies and detected using an ECL kit
626 (Beyotime, China, Cat#P0018S). The primary antibodies included Lamin B Polyclonal
627 antibody (Proteintech, China, Cat#12987-1-AP), GAPDH Monoclonal antibody (SCTB,
628 USA, Cat#sc-47724), CD84 Monoclonal antibody (Invitrogen, USA, Cat# MA5-42775),
629 Gclc Polyclonal antibody (Proteintech, China, Cat#12601-1-AP), Gclm Polycloncal
630 antibody (Proteintech, China, Cat#14241-1-AP), Ubiquitin Monoclonal antibody (Abclonal,
631 China, Cat#A19686), actin Monoclonal antibody (Proteintech, China, Cat#66009-1-Ig).

632 **Establishment of AML patient derived xenograft (PDX) for survival analysis**
633 **following CD84 knockdown.** AML PDX cells with luciferase reporter were generously
634 provided by Dr. Rui Su's laboratory at City of Hope (PDX-148)(63). Eight million cells were
635 equally divided and transduced with human shCtrl and shCD84 lentiviral particles at MOI
636 = 20 with TransDux MAX^{TM} reagent (System Biosciences, catalog # LV860A-1) following
637 manufacturer's protocol with no modifications for non-adherent cells. Following 2 hours
638 of spinoculation, cells were immediately injected into NSG mice and tumor burden

639 monitored by bioluminescence imaging weekly. Around 200,000 cells were cultured ex
640 vivo of each treatment group to monitor CD84 knockdown.

641 ***Statistical analysis*** All statistical analyses were performed as indicated in each figure
642 using GraphPad Prism (v9) software. Unpaired Student's t-test was used to compare
643 between two groups. whereas one-way ANOVA with multiple comparisons was used to
644 compare multiple groups. The log-rank (Mantel-Cox) was used to assess statistical
645 significant differences in mice survival between treatment groups. A p value less than
646 0.05 was considered statistically significant（*p< 0.05; **p<0.01;***p<0.001, and ****
647 p<0.0001), and data are presented as mean ± SEM.

648 ***Study Approval*** All animal protocols were approved by the Animal Care and Use
649 Committee of the City of Hope National Medical Center, in accordance with the National
650 Institute of Health Guidelines for the Care and Use of Laboratory Animals. NSG and
651 C57BL/6 mice were obtained through animal breeding facility at City of Hope and CD45.1
652 mice (B6-Ly5.1) were purchased from Charles River laboratories. Frozen PB MNCs from
653 AML patients were obtained from the City of Hope (COH) Hematopoietic Tissue
654 Biorepository IRB#18067. All patient characteristics are summarized in Supplementary
655 Table 1. Sample acquisition was approved by the COH Institutional Review Board in
656 accordance with the Declaration of Helsinki. Written informed consent was received from
657 all participants prior to inclusion in the study. Healthy donor PBMCs were obtained from
658 a leukocyte filter collected through healthy platelet donors at the COH blood donor center.

659

660 **Data availability**

661 All primary data will be made available upon reasonable request by emailing the two
662 corresponding authors. The bulk RNA-seq data that support this study has been
663 deposited in the Gene Expression Omnibus under accession no. GSE288016.

664 **Acknowledgments**

665 We thank to Dr. Idit Shachar, Weizmann Institute of Science, Rehovot, Israel for her
666 scientific support in investigating CD84. We are grateful to Tinisha McDonald, Kelly
667 Synold, and Elena Pulkinen for technical support in this work. We thank Dr. Jianjun Chen
668 for providing AML PDX cells. Research reported in this publication was in part supported
669 by an International Collaboration Grant from the Jacki and Bruce Barron Cancer
670 Research Scholars' Program, a partnership of the ICRF and City of Hope, as supported
671 by The Harvey L. Miller Family Foundation (FP, IS). This research was partially supported
672 by the National Institutes of Health grant R50-CA252135 (EC). This research was partially
673 supported by Key Research and Development Program of Zhejiang Province, China
674 (2024C03162). Research reported in this publication included work performed at the City
675 of Hope Liquid Tissue Bank, Mass Spectrometry and Proteomics Core Facility, Analytical
676 Cytometry, Small Imaging and Drug Discovery and Structural Biology cores supported by
677 the National Institutes of Health under award number P30CA033572. The content is
678 solely the responsibility of the authors and does not represent the official views of the
679 National Cancer Institute or the National Institutes of Health.

680 **Authorship Contributions**

681 YZ designed experiments, interpreted results, wrote the manuscript, and performed
682 experiments, including GEO database analysis, gene editing, mice experiment, RNA-seq

683 and flow cytometry, based on her extended contribution in the manuscript writing and on
684 her experimental work she is listed as first co-first author; MM-performed experiments
685 including AML cell line and PDX xenografts, MLL-AF9 and inv(16) c-kit transduction, flow
686 cytometry, colony formation, CD84 mRNA and protein correlation analysis, wrote part of
687 the methods and figure legend sections.; She also scientifically edited the manuscript, for
688 this reason she is listed as second co-first author; ML performed mechanism studies and
689 scientifically edited the manuscript but did not contribute in the writing; for this reason she
690 is listed as the 3rd co-first author of the manuscript; EC conducted mouse experiments;
691 ON-performed the CD84 supported with mice transplantation and colony assays; LXTN
692 performed seahorse assay and electron microscope experiment; HW collected AML
693 primary patients sample; MM, LN, -conducted health donor and AML patient samples; TT
694 performed CyTOF analysis; XW and MM collected AML primary patients sample and
695 analyzed the data of CD84 expression in AML; AP assisted in statistical analysis; RS
696 provided the mouse AML cells; XL performed flow cytometry of CD84 expression in AML
697 primary cells; MDE prepared for mice experiments; RP, JS performed the IHC staining of
698 normal tissue and AML patient samples; JFS revised the manuscript; LZ, ML and YF-
699 provided inv(16) mice pre-leukemia cells; BA, LL, Y-HK and SR-reviewed manuscript;
700 GM-supported the experimental design and reviewed the manuscript; JCW supported the
701 experimental design and contributed to the manuscript writing; FP supported, designed,
702 directed and, review the study and wrote the manuscript; FP and YZ prepared the
703 manuscript with input from other authors.

704

705 **Conflict of interest statement**

706 SR is a founder and member of the Scientific Advisory Board of Slam Bio Tx. JCW and
707 FP are consultants to Slam Bio Tx. The studies reported were performed and supported
708 independently of Slam Bio Tx.

709

710

711 **References**

712 1. Kantarjian H, et al. Acute myeloid leukemia: current progress and future directions.
713 *Blood Cancer J.* 2021;11(2):41.
714 2. Masetti R, Baccelli F, Leardini D, and Locatelli F. Venetoclax: a new player in the
715 treatment of children with high-risk myeloid malignancies? *Blood advances.*
716 2024;8(13):3583-95.
717 3. Shimony S, Stahl M, and Stone RM. Acute myeloid leukemia: 2023 update on diagnosis,
718 risk-stratification, and management. *American journal of hematology.* 2023;98(3):502-26.
719 4. Kumar CC. Genetic abnormalities and challenges in the treatment of acute myeloid
720 leukemia. *Genes & cancer.* 2011;2(2):95-107.
721 5. Mattes K, Vellenga E, and Schepers H. Differential redox-regulation and mitochondrial
722 dynamics in normal and leukemic hematopoietic stem cells: A potential window for
723 leukemia therapy. *Critical reviews in oncology/hematology.* 2019;144:102814.
724 6. Zhang BB, Wang DG, Guo FF, and Xuan C. Mitochondrial membrane potential and
725 reactive oxygen species in cancer stem cells. *Familial cancer.* 2015;14(1):19-23.
726 7. Schieber M, and Chandel NS. ROS function in redox signaling and oxidative stress.
727 *Current biology : CB.* 2014;24(10):R453-62.
728 8. Snezhkina AV, et al. ROS Generation and Antioxidant Defense Systems in Normal and
729 Malignant Cells. *Oxidative medicine and cellular longevity.* 2019;2019:6175804.
730 9. Trombetti S, et al. Oxidative Stress and ROS-Mediated Signaling in Leukemia: Novel
731 Promising Perspectives to Eradicate Chemoresistant Cells in Myeloid Leukemia.
732 *International journal of molecular sciences.* 2021;22(5).
733 10. Yu X, et al. Inhibition of NRF2 enhances the acute myeloid leukemia cell death induced
734 by venetoclax via the ferroptosis pathway. *Cell death discovery.* 2024;10(1):35.

735 11. Hu T, et al. Nrf2 overexpression increases the resistance of acute myeloid leukemia to
736 cytarabine by inhibiting replication factor C4. *Cancer gene therapy.* 2022;29(11):1773-
737 90.
738 12. Martelli AM, et al. Phosphoinositide 3-kinase/Akt signaling pathway and its therapeutical
739 implications for human acute myeloid leukemia. *Leukemia.* 2006;20(6):911-28.
740 13. Li W, and Kong AN. Molecular mechanisms of Nrf2-mediated antioxidant response.
741 *Molecular carcinogenesis.* 2009;48(2):91-104.
742 14. Panieri E, et al. Potential Applications of NRF2 Modulators in Cancer Therapy.
743 *Antioxidants (Basel, Switzerland).* 2020;9(3).
744 15. Darici S, Alkhaldi H, Horne G, Jørgensen HG, Marmiroli S, and Huang X. Targeting
745 PI3K/Akt/mTOR in AML: Rationale and Clinical Evidence. *Journal of clinical medicine.*
746 2020;9(9).
747 16. Agod Z, et al. Signaling Lymphocyte Activation Molecule Family 5 Enhances Autophagy
748 and Fine-Tunes Cytokine Response in Monocyte-Derived Dendritic Cells via
749 Stabilization of Interferon Regulatory Factor 8. *Front Immunol.* 2018;9:62.
750 17. Lewinsky H, et al. CD84 is a regulator of the immunosuppressive microenvironment in
751 multiple myeloma. *JCI Insight.* 2021;6(4).
752 18. Yan Q, et al. Structure of CD84 provides insight into SLAM family function. *Proceedings*
753 *of the National Academy of Sciences of the United States of America.*
754 2007;104(25):10583-8.
755 19. Martin M, et al. CD84 functions as a homophilic adhesion molecule and enhances IFN-
756 gamma secretion: adhesion is mediated by Ig-like domain 1. *J Immunol.*
757 2001;167(7):3668-76.
758 20. Lewinsky H, et al. CD84 regulates PD-1/PD-L1 expression and function in chronic
759 lymphocytic leukemia. *J Clin Invest.* 2018;128(12):5465-78.

760 21. Binsky-Ehrenreich I, et al. CD84 is a survival receptor for CLL cells. *Oncogene.*
761 2014;33(8):1006-16.
762 22. Wei Y, et al. Targeting Bcl-2 Proteins in Acute Myeloid Leukemia. *Frontiers in oncology.*
763 2020;10:584974.
764 23. Alshetaiwi H, et al. Defining the emergence of myeloid-derived suppressor cells in breast
765 cancer using single-cell transcriptomics. *Sci Immunol.* 2020;5(44).
766 24. Kim Y, et al. Terminal deoxynucleotidyl transferase and CD84 identify human multi-
767 potent lymphoid progenitors. *Nature communications.* 2024;15(1):5910.
768 25. Thomas D, and Majeti R. Biology and relevance of human acute myeloid leukemia stem
769 cells. *Blood.* 2017;129(12):1577-85.
770 26. Tsherniak A, et al. Defining a Cancer Dependency Map. *Cell.* 2017;170(3):564-76 e16.
771 27. Gentles AJ, et al. The prognostic landscape of genes and infiltrating immune cells
772 across human cancers. *Nature medicine.* 2015;21(8):938-45.
773 28. Győrffy B. Integrated analysis of public datasets for the discovery and validation of
774 survival-associated genes in solid tumors. *Innovation (Cambridge (Mass)).*
775 2024;5(3):100625.
776 29. Tyner JW, et al. Functional genomic landscape of acute myeloid leukaemia. *Nature.*
777 2018;562(7728):526-31.
778 30. Kuo YH, et al. Cbf beta-SMMHC induces distinct abnormal myeloid progenitors able to
779 develop acute myeloid leukemia. *Cancer Cell.* 2006;9(1):57-68.
780 31. Perelman A, Wachtel C, Cohen M, Haupt S, Shapiro H, and Tzur A. JC-1: alternative
781 excitation wavelengths facilitate mitochondrial membrane potential cytometry. *Cell Death*
782 *Dis.* 2012;3(11):e430.
783 32. Wang M, et al. Exogenous H(2)S initiating Nrf2/GPx4/GSH pathway through promoting
784 Syvn1-Keap1 interaction in diabetic hearts. *Cell death discovery.* 2023;9(1):394.

785 33. Adinolfi S, et al. The KEAP1-NRF2 pathway: Targets for therapy and role in cancer.
786 *Redox biology.* 2023;63:102726.
787 34. Giustarini D, Dalle-Donne I, Milzani A, Fanti P, and Rossi R. Analysis of GSH and GSSG
788 after derivatization with N-ethylmaleimide. *Nature protocols.* 2013;8(9):1660-9.
789 35. Xue Z, Nuerrula Y, Sitiwaerdi Y, and Eli M. Nuclear factor erythroid 2-related factor 2
790 promotes radioresistance by regulating glutamate-cysteine ligase modifier subunit and
791 its unique immunoinvasive pattern. *Biomolecules & biomedicine.* 2024;24(3):545-59.
792 36. He F, et al. NRF2 activates growth factor genes and downstream AKT signaling to
793 induce mouse and human hepatomegaly. *Journal of hepatology.* 2020;72(6):1182-95.
794 37. Lee JM, Hanson JM, Chu WA, and Johnson JA. Phosphatidylinositol 3-kinase, not
795 extracellular signal-regulated kinase, regulates activation of the antioxidant-responsive
796 element in IMR-32 human neuroblastoma cells. *The Journal of biological chemistry.*
797 2001;276(23):20011-6.
798 38. Nakaso K, Yano H, Fukuhara Y, Takeshima T, Wada-Isoe K, and Nakashima K. PI3K is
799 a key molecule in the Nrf2-mediated regulation of antioxidative proteins by hemin in
800 human neuroblastoma cells. *FEBS letters.* 2003;546(2-3):181-4.
801 39. Li MH, Cha YN, and Surh YJ. Peroxynitrite induces HO-1 expression via PI3K/Akt-
802 dependent activation of NF-E2-related factor 2 in PC12 cells. *Free radical biology &*
803 *medicine.* 2006;41(7):1079-91.
804 40. Kubben N, et al. Repression of the Antioxidant NRF2 Pathway in Premature Aging. *Cell.*
805 2016;165(6):1361-74.
806 41. Dhakshinamoorthy S, and Jaiswal AK. Functional characterization and role of INrf2 in
807 antioxidant response element-mediated expression and antioxidant induction of
808 NAD(P)H:quinone oxidoreductase1 gene. *Oncogene.* 2001;20(29):3906-17.

809 42. Satoh T, et al. Activation of the Keap1/Nrf2 pathway for neuroprotection by electrophilic
810 [correction of electrophillic] phase II inducers. *Proceedings of the National Academy of*
811 *Sciences of the United States of America.* 2006;103(3):768-73.
812 43. Sintes J, Romero X, de Salort J, Terhorst C, and Engel P. Mouse CD84 is a pan-
813 leukocyte cell-surface molecule that modulates LPS-induced cytokine secretion by
814 macrophages. *J Leukoc Biol.* 2010;88(4):687-97.
815 44. Zhang Q, et al. Activation of RAS/MAPK pathway confers MCL-1 mediated acquired
816 resistance to BCL-2 inhibitor venetoclax in acute myeloid leukemia. *Signal Transduct*
817 *Target Ther.* 2022;7(1):51.
818 45. Platanias LC. Map kinase signaling pathways and hematologic malignancies. *Blood.*
819 2003;101(12):4667-79.
820 46. Ling Q, et al. MAP4K1 functions as a tumor promotor and drug mediator for AML via
821 modulation of DNA damage/repair system and MAPK pathway. *EBioMedicine.*
822 2021;69:103441.
823 47. Sapienza MR, et al. Molecular profiling of blastic plasmacytoid dendritic cell neoplasm
824 reveals a unique pattern and suggests selective sensitivity to NF-kB pathway inhibition.
825 *Leukemia.* 2014;28(8):1606-16.
826 48. Zhou J, Ching YQ, and Chng WJ. Aberrant nuclear factor-kappa B activity in acute
827 myeloid leukemia: from molecular pathogenesis to therapeutic target. *Oncotarget.*
828 2015;6(8):5490-500.
829 49. Bosman MC, Schuringa JJ, and Vellenga E. Constitutive NF-kappaB activation in AML:
830 Causes and treatment strategies. *Crit Rev Oncol Hematol.* 2016;98:35-44.
831 50. Yan D, et al. Sirt5 Is a Druggable Metabolic Vulnerability in Acute Myeloid Leukemia.
832 *Blood Cancer Discov.* 2021;2(3):266-87.
833 51. Kumar B. Harnessing the Metabolic Vulnerabilities of Leukemia Stem Cells to Eradicate
834 Acute Myeloid Leukemia. *Front Oncol.* 2021;11:632789.

835 52. de Beauchamp L, Himonas E, and Helgason GV. Mitochondrial metabolism as a
836 potential therapeutic target in myeloid leukaemia. *Leukemia.* 2022;36(1):1-12.
837 53. Peng M, Huang Y, Zhang L, Zhao X, and Hou Y. Targeting Mitochondrial Oxidative
838 Phosphorylation Eradicates Acute Myeloid Leukemic Stem Cells. *Front Oncol.*
839 2022;12:899502.
840 54. Tcheng M, et al. Very long chain fatty acid metabolism is required in acute myeloid
841 leukemia. *Blood.* 2021;137(25):3518-32.
842 55. Farge T, et al. Chemotherapy-Resistant Human Acute Myeloid Leukemia Cells Are Not
843 Enriched for Leukemic Stem Cells but Require Oxidative Metabolism. *Cancer discovery.*
844 2017;7(7):716-35.
845 56. Khorashad JS, Rizzo S, and Tonks A. Reactive oxygen species and its role in
846 pathogenesis and resistance to therapy in acute myeloid leukemia. *Cancer drug*
847 *resistance (Alhambra, Calif).* 2024;7:5.
848 57. Chen Y, Liang Y, Luo X, and Hu Q. Oxidative resistance of leukemic stem cells and
849 oxidative damage to hematopoietic stem cells under pro-oxidative therapy. *Cell Death*
850 *Dis.* 2020;11(4):291.
851 58. Lagadinou ED, et al. BCL-2 inhibition targets oxidative phosphorylation and selectively
852 eradicates quiescent human leukemia stem cells. *Cell Stem Cell.* 2013;12(3):329-41.
853 59. Susnow N, Zeng L, Margineantu D, and Hockenbery DM. Bcl-2 family proteins as
854 regulators of oxidative stress. *Seminars in cancer biology.* 2009;19(1):42-9.
855 60. Huang J, Zhao Y, Zhao K, Yin K, and Wang S. Function of reactive oxygen species in
856 myeloid-derived suppressor cells. *Frontiers in immunology.* 2023;14:1226443.
857 61. Veglia F, Sanseviero E, and Gabrilovich DI. Myeloid-derived suppressor cells in the era
858 of increasing myeloid cell diversity. *Nature reviews Immunology.* 2021;21(8):485-98.
859 62. Ohl K, et al. Nrf2 Is a Central Regulator of Metabolic Reprogramming of Myeloid-Derived
860 Suppressor Cells in Steady State and Sepsis. *Frontiers in immunology.* 2018;9:1552.

861 63. Lu J, Zhao H, Yang L, and Jiang X. Protocol to establish a stable MLL-AF9_AML mouse
862 model. *STAR protocols.* 2022;3(3):101559.

863

864

865 **Figures and figure legends**

Figure 1

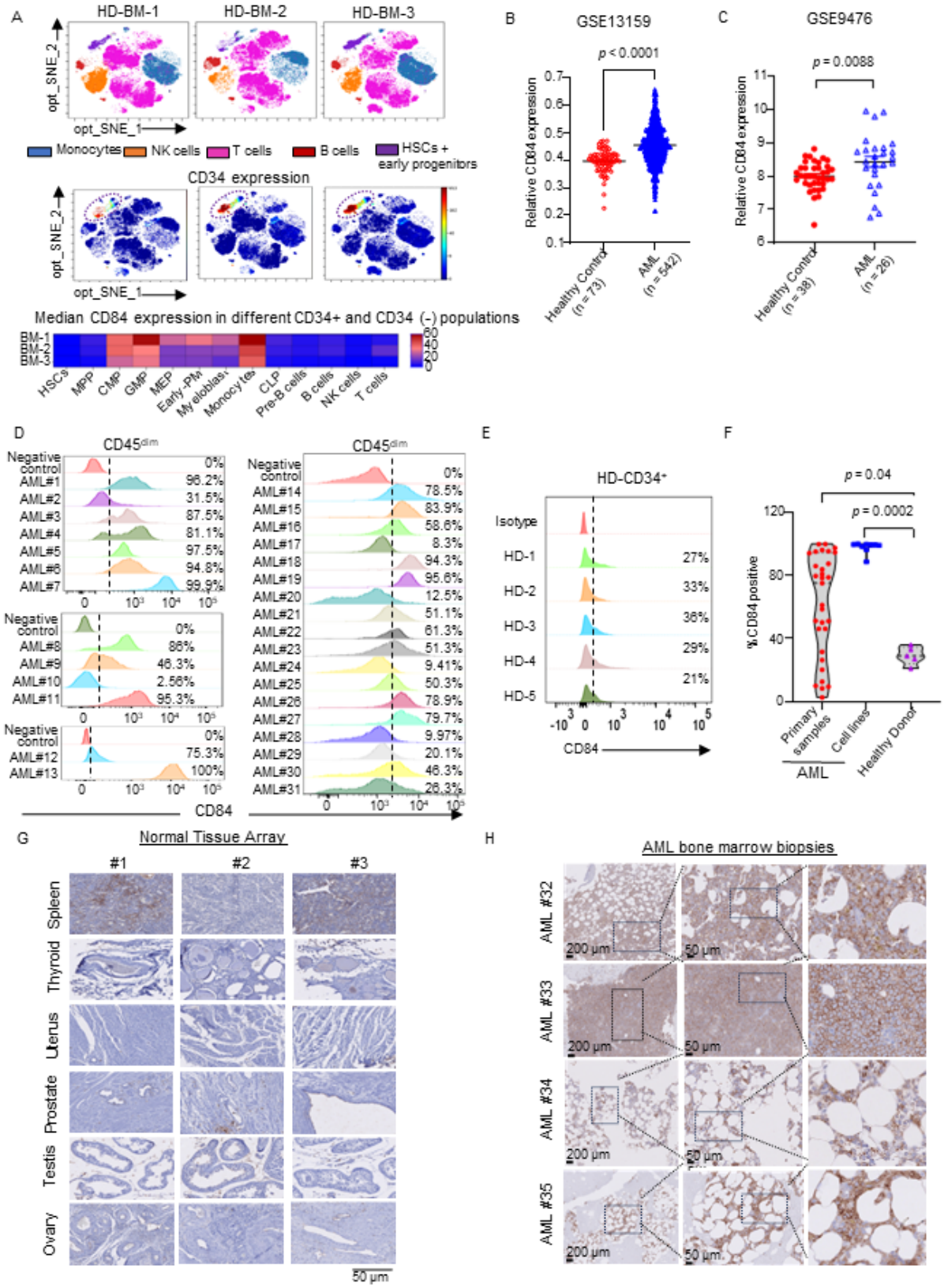
A
HD-BM-1
HD-BM-2
HD-BM-3
opt_SNE_2
opt_SNE_1
Monocytes
NK cells
T cells
B cells
HSCs + early progenitors
CD34 expression
Median CD84 expression in different CD34+ and CD34 (-) populations
BM-1
BM-2
BM-3
HSCs
MPP
CMP
GMP
MEP
Early-PM
Myeloblast
Monocytes
CLP
Pre-B cells
B cells
NK cells
T cells
B
GSE13159
p < 0.0001
Relative CD84 expression
Healthy Control (n = 73)
AML (n = 542)
C
GSE9476
p = 0.0088
Healthy Control (n = 38)
AML (n = 26)
D
CD45dim
Negative control
AML#1
AML#2
AML#3
AML#4
AML#5
AML#6
AML#7
AML#8
AML#9
AML#10
AML#11
AML#12
AML#13
AML#14
AML#15
AML#16
AML#17
AML#18
AML#19
AML#20
AML#21
AML#22
AML#23
AML#24
AML#25
AML#26
AML#27
AML#28
AML#29
AML#30
AML#31
CD84
E
HD-CD34+
Isotype
HD-1
HD-2
HD-3
HD-4
HD-5
CD84
F
p = 0.04
p = 0.0002
% CD84 positive
Primary samples
Cell lines
Healthy Donor
AML
G
Normal Tissue Array
#1
#2
#3
Spleen
Thyroid
Uterus
Prostate
Testis
Ovary
50 µm
H
AML bone marrow biopsies
AML #32
AML #33
AML #34
AML #35
200 µm
50 µm

866

867 **Figure 1. CD84 is overexpressed in AML**. **(A)** Bone marrow cells were subjected to
868 CyTOF immunophenotyping comprising 39 surface markers tailored to detect different
869 immune subsets. Analysis was performed with Cytobank© platform in independent
870 healthy donors (n=3). **(B)** Scatter plots of CD84 messenger RNA (mRNA) expression in
871 bone marrow mononuclear cells from patients with AML (n=542) and healthy donors
872 (n=73) (from GSE13159 dataset) indicating increased CD84 expression in AML
873 specimens. Graph are presentated as mean ± standard error of the mean (SEM)
874 Statistical significance was assessed by two tailed unpaired t test. (**C**) Scatter plots of
875 CD84 messenger RNA (mRNA) expression in leukemia blasts from patients with AML
876 (n=26) and CD34+ cells isolated from healthy donors (n=38) (from GSE9476 dataset)
877 indicating increased CD84 expression in AML specimens. Graph are presentated as
878 mean ± SEM. Statistical significance was assessed by two tailed unpaired t test. (**D**)
879 Histogram showing CD84 surface protein expression in different AML patient specimens
880 (n=31) as analyzed by flow cytometry, highlighting that CD84 is highly expressed in AML
881 primary patient cells. PE anti-human CD84 (clone CD84.1.21; Biolegend) was used (1
882 µl/test). (**E**) Histogram showing flow cytometry profiles of CD84 expression in healthy
883 donors CD34+ cellularr population. The analysis was conducted in independent donors
884 (n=5). (**F**) Violin plot shown the percentage of CD84 expressing cells among AML primary
885 patients (n=31), AML cell lines (n=9) and healthy donor cells (n=5). Data are presentated
886 as mean ± SEM. Statistical significance was assessed by one-way ANOVA. (**G**)
887 Representative images of immunohistochemical staining of CD84 performed in normal
888 tissue array. Each normal tissue stained for CD84 was obtained from a minimum of three
889 independent normal donors. Scale bar: 50 µm. (**H**) Representative images of

890 immunohistochemical staining of CD84 in AML bone marrow. The images are magnified
891 at 200X, scale bar: 200 μm. The analysis was conducted in 15 independent AML donor
892 biopses (see also Figure S2G).

893

Figure 2

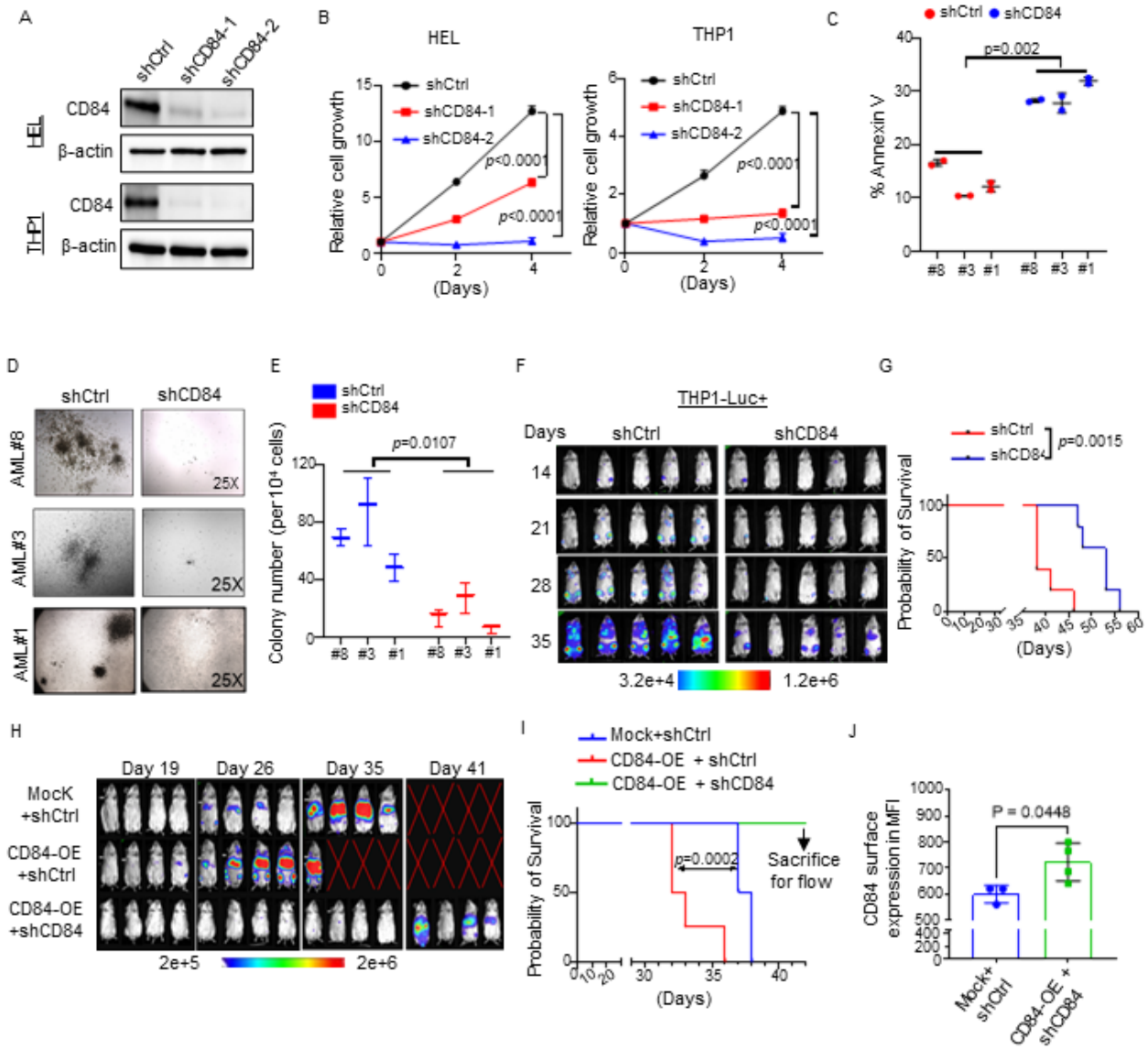

894

895 **Figure 2. CD84 deletion dampens AML survival in both AML cell lines and cell**
896 **derived xenogtaft.** (**A**) Western blot of the indicated proteins in THP1 cells and HEL cells
897 transduced with two shRNAs against CD84 (shCD84-1; shCD84-2) or scramble control
898 (shCtrl). Data are representative of at least 2 independent experiments. (**B**) Connecting
899 line graph representing cell proliferative analysis of THP-1 cells and HEL cells transduced

900 with shCtrl or shCD84 lentiviral vectors. Data are presented as mean ± SEM and are
901 representative of 3 biological replicates. Statistical significance was assessed by two-way
902 ANOVA (mix model). (**C**) Bar chart showing apoptosis levels indicated by Annexin-
903 APC/DAPI in three AML patient specimens transduced with shCtrl or shCD84 lentiviral
904 vector. Data are presented as mean ± SEM and are representative of 3 independent
905 experiments. Statistical significance was assessed by two-way ANOVA. (**D-E**) AML cells
906 obtained from three different donors(AML #1, #3, #8) were transduced with shCtrl or
907 shCD84 lentivirus. Representative colony images are in Figure 2D. The graph in Figure
908 2E shows AML colony formation cell (CFC) frequencies after 10 days of culture. Data are
909 presented as mean ± SEM and are representative of 3 biological replicates. Statistical
910 significance was assessed by two-way ANOVA. (n=3 independentreplicates per sample).
911 (**F**) Bioluminescent imaging showing the tumor burden in xenograft NSG mice on days
912 14-35 following shCtrl or shCD84–transduced THP1-luciferase cell transplantation (n=5
913 per group). (**G**) Kaplan-Meier analysis of survival of THP1-luciferase cell (shCtrl or
914 shCD84) transplanted NSG mice. Each group consisted of 5 mice. Statistical significance
915 was assessed by log-rank test. (**H**) Bioluminescent imaging showing the tumor burden in
916 xenograft NSG mice on days 19-41 following mock/shCtrl, CD84-OE/shCtrl or CD84-
917 OE/shCD84–transduced THP1-luciferase cell transplantation (n=4 per group). (**I**) Kaplan-
918 Meier analysis of survival of THP1-luciferase cell (mock/shCtrl, CD84-OE/shCtrl or CD84-
919 OE/shCD84) transplanted NSG mice (n=4 per group). Statistical significance was
920 assessed by log-rank test. (**J**) Bar chart shown the CD84 surface expression in bone
921 marrow cells from NSG mice xenografted with THP1 luciferase cells transduced with

922 mock/shCtrl or CD84-OE/shCD84. Data are presented as mean ± SEM and each dot
923 reppresents 1 mouse. Statistical significance was assessed by two tailed unpaired t test.
924

Figure 3

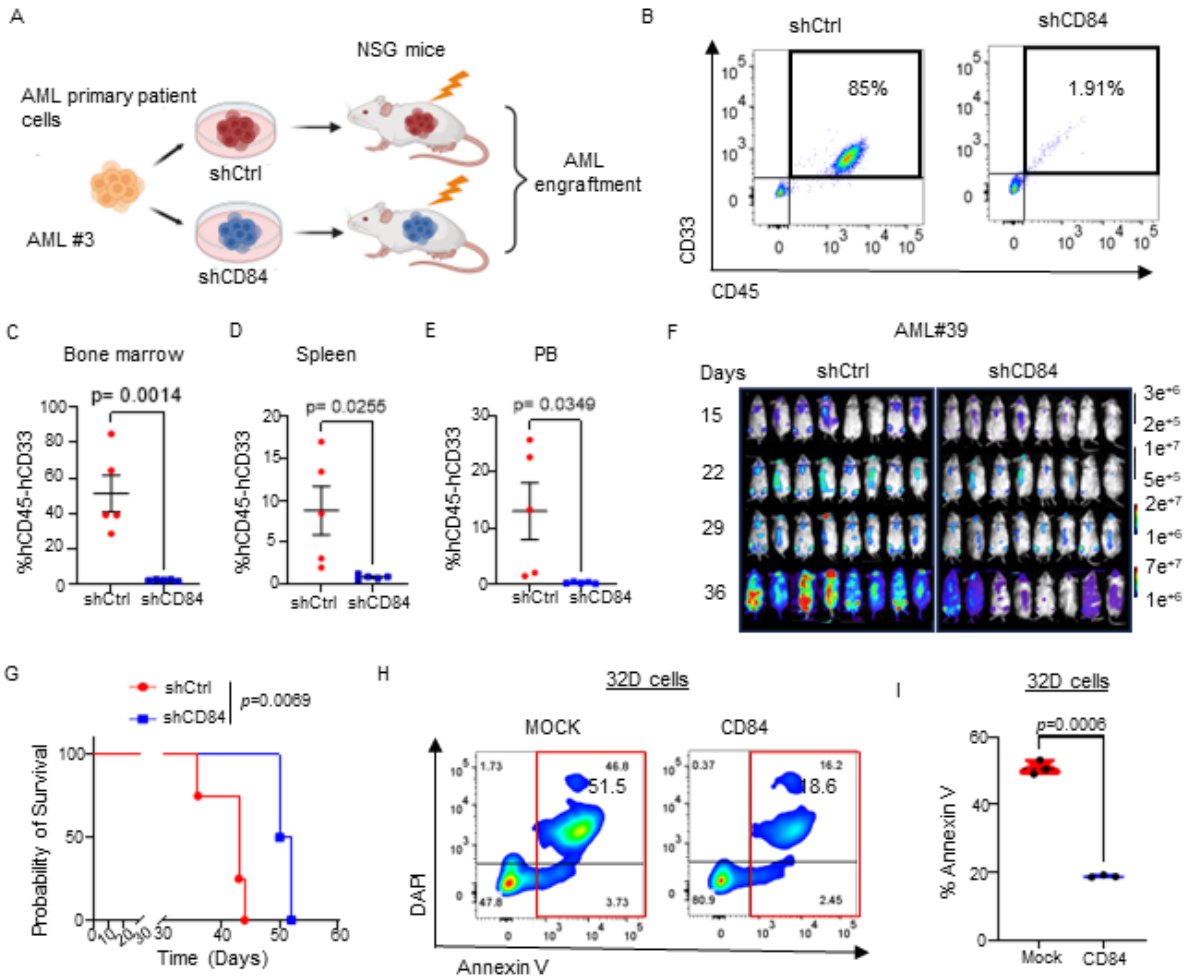

925

926 **Figure 3. CD84 loss impairs AML development in patient-derived xenograft.** (**A**)
927 Scheme of the design and procedures of generating a CD84-knockdown, AML patient-
928 derived xenograft model. AML primary patient cells were transduced with shCtrl or
929 shCD84 lentivirus. After puromycin selection, shCtrl or shCD84 AML primary cells were
930 injected into irradiated NSG mice. (**B**) Representative flow cytometry profile of human
931 AML cells (human CD45+/CD33+) engrafted in BM. (**C-E**) Scatter plots showing the
932 percentage of human AML cells (human CD45+/CD33+) engrafted in BM (C), spleen (D),
933 and peripheral blood (PB) (E) of recipient NSG mice (n=5 per group). Data are presented

934 as mean ± SEM and are representative of 5 individual mice per group. Statistical
935 significance was assessed by two tailed unpaired t test. (**F**) Bioluminescent imaging
936 showing the tumor burden in xenograft NSG mice (frontal and dorsal) following shCtrl or
937 shCD84–transduced AML PDX-luciferase cell transplantation (n=4 per group). (**G**)
938 Kaplan-Meier survial analysis of AML PDX-luciferase cell (shCtrl or shCD84) transplanted
939 NSG mice (n=4 per group). Statistical significance was assessed by log-rank test. (**H**)
940 Flow cytometry profile showing apoptosis levels indicated by Annexin-APC/DAPI in 32D
941 cells transfected with lentivirus including CD823-mock vector or CD823-CD84 WT. (**I**)
942 Violin plot showing apoptosis levels indicated by Annexin V-APC/DAPI in 32D cells
943 transduced with Mock or CD84-WT. Data are presented as mean ± SEM and are
944 representative of 3 biological replicates. Statistical significance was assessed by two
945 tailed unpaired t test.

946

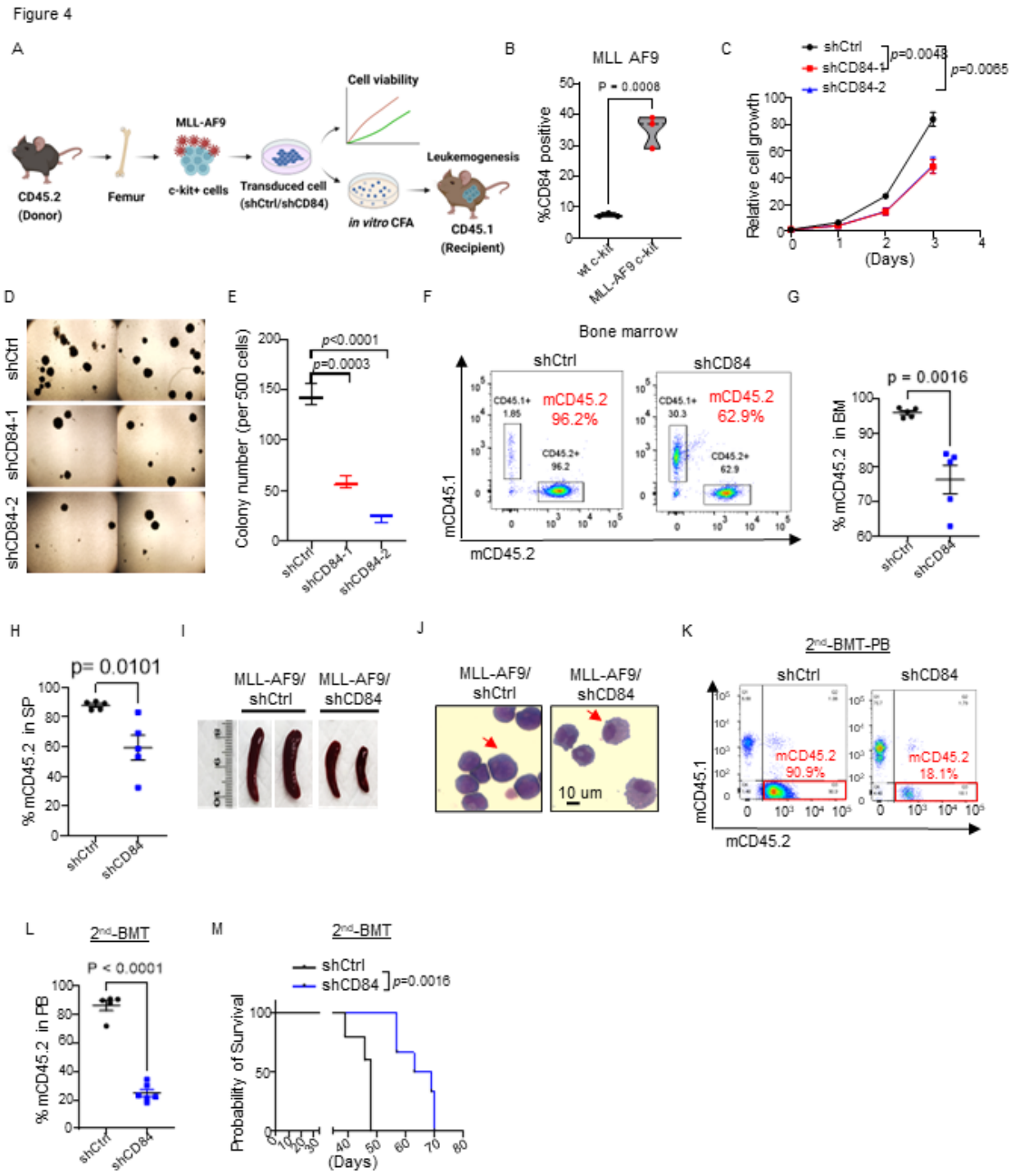

Figure 4. CD84 is essential for AML maintenance in MLL-AF9 mouse model *in vivo*. (**A**) Scheme of the design and procedures of generating an MLL-AF9 AML mice model with CD84 knockdown. c-kit+ cells were isolated from C57BL/6J CD45.2 mice, which

951 were co-transduced with MLL-AF9 retroviruses. GFP+ MLL-AF9 AML cells were sorted
952 and transfected with shCtrl or shCD84-1/shCD84-2 lentivirus. After puromycin selection,
953 assays were performed with pre-leukemic MLL-AF9 cells with the indicated vectors,
954 including a cell proliferation assay and a colony formation cell assay. The cells harvested
955 from the colony formation cell assay were transplanted into CD45.1 C57BL/6 mice. (**B**)
956 Violin chart shown CD84 expression in c-kit+ cells before and post MLL-AF9 transduction.
957 Data are presented as mean ± SEM and are representative of 3 independent experiments.
958 Statistical significance was assessed by two tailed unpaired t test. (**C**) Connecting line
959 graph representing cell proliferative analysis of MLL-AF9 AML cells transduced with
960 shCtrl or shCD84 (shCD84-1; shCD84-2) lentiviral vector. Data are presented as mean ±
961 SEM and are representative of 3 independent experiments. Statistical significance was
962 assessed by two-way ANOVA (mixed model). (**D**) Representative colony formation
963 images of MLL-AF9 c-kit+ cells transduced with shCtrl or shCD84 (shCD84-1; shCD84-
964 2). Images were acquired in tiles by the City of Hope microscopy core facility using ZEN
965 3.1 (blue edition, Carl Zeiss Microscopy GmbH); (**E**) The graph shows MLL-AF9 AML
966 colony formation cell numbers after 7 days of culture. Data are presented as mean ± SEM
967 and are representative of 3 independent experiments. Statistical significance was
968 assessed by one way ANOVA. (**F**) Reppresentative scatter plots showing the percentage
969 of donor cells (mouse CD45.2), transduced with shCtrl or shCD84 and engrafted in the
970 bone marrow (BM); (G-H) Graphs showing the % of mouse mouse CD45.2 in the BM (G)
971 and)spleen (H) of recipient mice (mouse CD45.1), at around 5 weeks after BM
972 transplantation (n=5 per group). Data are presented as mean ± SEM and are
973 representative of 5 individual mice. Statistical significance was assessed by two tailed

974 unpaired t test in Figure G and H. (**I**) Representative spleen image of recipient mice
975 xenografted with shCtrl-MLL-AF9 or shCD84-MLL-AF9. (**J**) Representative images of
976 Wright-Giemsa staining of BM from recipient mice transplanted with shCtrl-MLL-AF9 or
977 shCD84-MLL-AF9 AML cells (Red arrow indicates AML blast). (**K-L**) Reppresentative
978 scatter plot (K) and associated graph (L) showing the leukemic engraftment in the
979 peripheral blood (PB)of recipient mice (CD45.1) xenografted with MLL-AF9 AML with or
980 without CD84 silencing (CD45.2) upon secondary bone marrow transplantation (on day
981 38. Data are presented as mean ± SEM and are representative of at least 5 individual
982 mice per group. Statistical significance was assessed by two tailed unpaired t test. (**M**)
983 Kaplan-Meier analysis of survival of secondary bone marrow transplanted mice with MLL-
984 AF9 cells (shCtrl or shCD84) (n=5 per group). Statistical significance was assessed by
985 log-rank test.

986

Figure 5

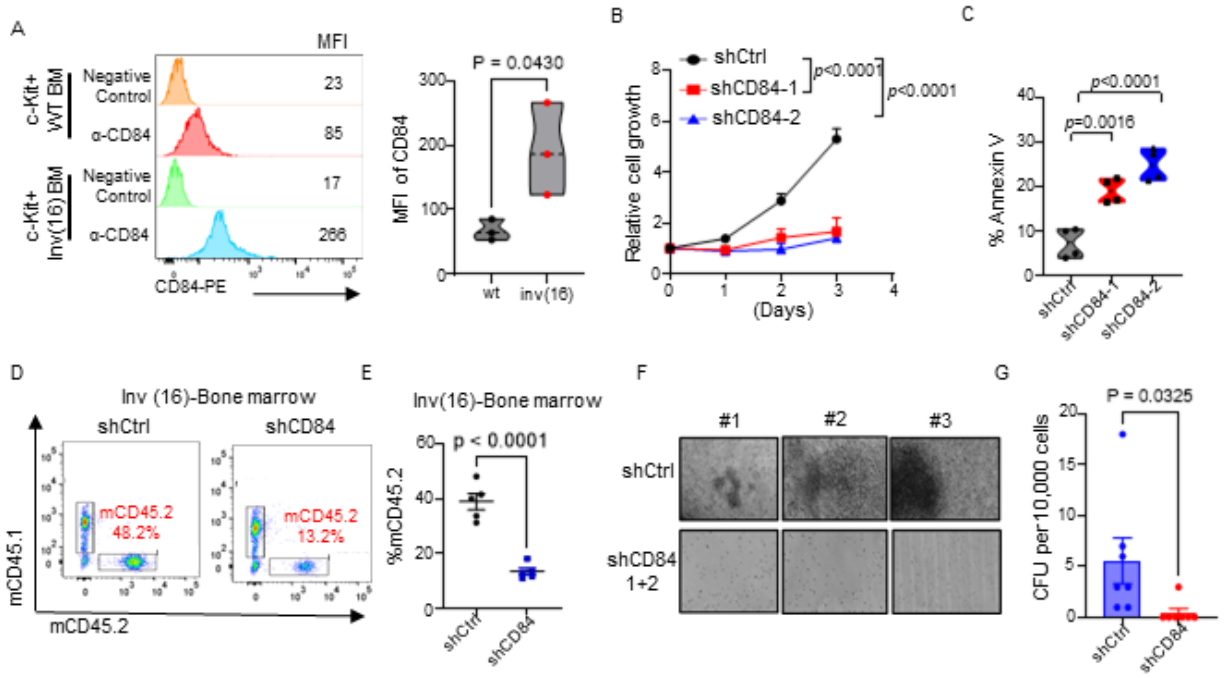

Figure 5. CD84 is essential for AML maintenance in inv(16) mouse model. (**A**) Histogram and violin chart shown CD84 expression in inv(16) c-kit+ cells, relative to wt c-kit+ cells. Data are presented as mean ± SEM and are representative of 3 independent experiments and mice. Statistical significance was assessed by two tailed unpaired t test. (**B**) Connecting line graph representing cell proliferative analysis of inv(16)-AML cells transduced with shCtrl or shCD84 (shCD84-1; shCD84-2) lentiviral vector. Data are presented as mean ± SEM and are representative of 3 independent experiments. Statistical significance was assessed two-way ANOVA (mixed model). (**C**) Violin plot showing apoptosis levels indicated by Annexin-APC/DAPI in inv(16)-AML cells transduced with shCtrl or shCD84 lentiviral vector. Data are presented as mean ± SEM and are representative of 4 independent experiments. Statistical significance was assessed by one way ANOVA. (**D**) Representative flow cytometry profile of donor cells

1000 (mouse CD45.2) engrafted in bone marrow from shCtrl-inv (16) or shCD84-inv (16)
1001 transplanted mice. (**E**) Scatter plot showing the leukemic engraftment in the BM of
1002 recipient mice (CD45.1) xenografted with inv (16) AML with or without CD84 silencing
1003 (CD45.2) (n=5 per group). Data are presented as mean ± SEM and are representative of
1004 5 individual mice. Statistical significance was assessed by two tailed unpaired t test. (**F**)
1005 Representative colony images of inv(16)-AML cells transduced with shCtrl or shCD84-
1006 1+2. (**G**) The bar graph shows colony formation numbers of inv(16) transduced with shCtrl
1007 or shCD84-1+2 after 7 days of culture. Data are presented as mean ± SEM and are
1008 representative of 7 independent replicates. Statistical significance was assessed by two
1009 tailed unpaired t test.

1010

Figure 6

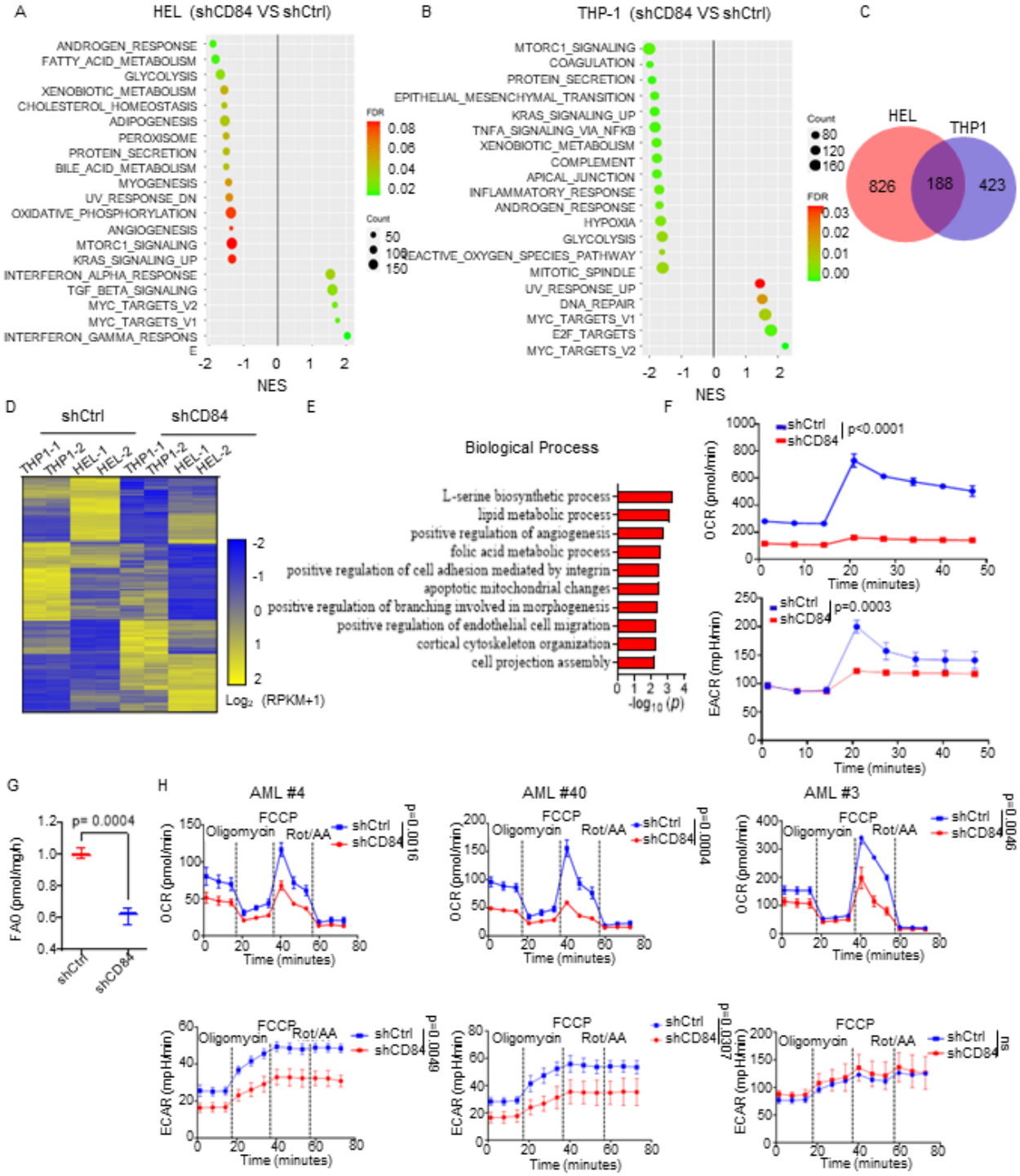

1011

1012 **Figure 6. CD84 knockdown deactivated energy metabolism and induced**

1013 **mitochondrial stress in AML.** (**A-B**) Scattergrams of CD84-related gene sets based on

1014 enrichment analyses of differentially expressed genes in HEL cells (shCD84 vs shCtrl)
1015 (**A**) and THP1 cells (shCD84 vs shCtrl) (**B**). The color indicates the false discovery rate q
1016 values; NES, normalized enrichment score. (**C**) Venn diagram showing the overlapped
1017 differentially expressed genes (DEGs) between HEL (shCD84 vs shCtrl) and THP1
1018 (shCD84 vs shCtrl) groups. (**D**) Heatmap showing gene expression of the overlapped
1019 differential genes between THP1 cells and HEL cells expressing shCD84 or shCtrl, based
1020 on a fold change >2/<0.5 and $p<0.05$. (**E**) Bar chart showing GO enrichment analysis of
1021 common differential expressed genes (DEGs; n=188) in two AML cell lines. (**F**)
1022 Connecting lines showing the effects of CD84 deletion on level of OCR and ECAR in
1023 THP1 cells. Cells were transfected with lentivirus expressing shCD84 or shCtrl, and
1024 puromycin selected for 2 days. The cells were harvested to measure levels of OCR and
1025 ECAR using the Seahorse XF cell energy phenotype test kit. Data are presented as mean
1026 ± SEM and are representative of 3 biological replicates. Statistical significance was
1027 assessed two-way ANOVA (mixed model). (**G**) Box chart showing the effects of CD84
1028 knockdown on FAO levels in THP1 cells. The cells were harvested as described in figure
1029 F, and FAO assay results are presented as fold change, compared to control. Data are
1030 presented as mean ± SEM and are representative of 3 independent experiments.
1031 Statistical significance was assessed by two tailed unpaired t test. (**H**) Connecting lines
1032 showing the effects of CD84 deletion on level of OCR and ECAR in primary AML cells
1033 obtaoined fron n=3 different donors. Cells were transduced with lentivirus expressing
1034 shCD84 or shCtrl for 48 hours. The cells were harvested to measure levels of OCR and
1035 ECAR using the Seahorse XF cell energy phenotype test kit. Data are presented as mean

1036 ± SEM and are representative of 3 independent experiments. Statistical significance was

1037 assessed two-way ANOVA (mixed model).

1038

Figure 7

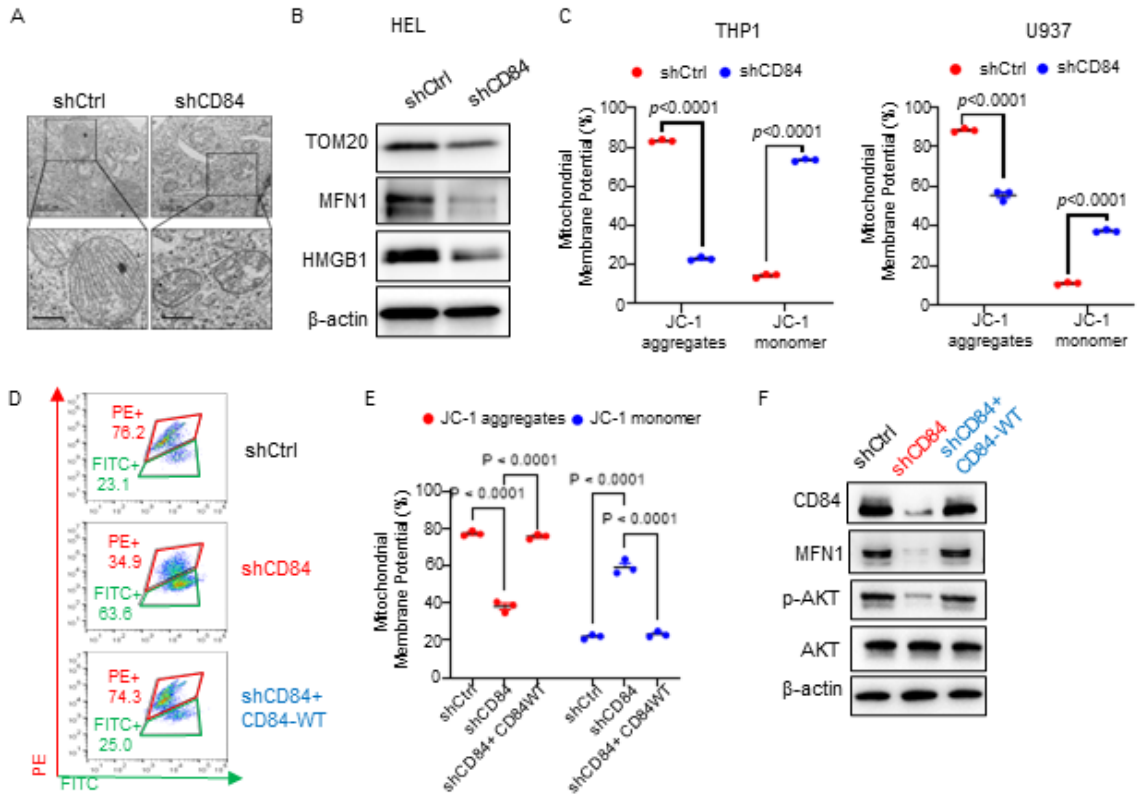

Figure 7. Knockdown of CD84 triggers mitochondrial stress in AML cells. (**A**) Representative images of transmission electron microscopy images of mitochondrial cristae in HEL cells transfected with shCtrl or shCD84 lentivirus. Scale bar, 1 μm (up), 0.5 μm (bottom). The analysis was conducted in at least 2 independent experimental sets. (**B**) Western blot of indicated proteins were performed in HEL cells transduced with lentivirus expressing either shCtrl or shCD84, indicating mitochondrial dysfunction in CD84 knockdown cells. Data are representative of 2 independent bilogical replicates. (**C**) Interleaved scatter plot showing the mitochondrial membrane potentials which were measured using JC-1 dye for flow cytometry. Data are presented as mean ± SEM and are representative of 3 independent experiments. Statistical significance was assessed

1050 by two tailed unpaired t test. (**D**) Representative flow cytometry profiles of JC-1 stained
1051 THP1, which were transduced with lentiviruses expressing indicated vectors (shCD84
1052 targeting 3'-UTR). Red (PE): Green (FITC) represents the monomers to aggregated ratio.
1053 (**E**) Interleaved scatter plot summarizing the alteration of mitochondrial membrane
1054 potentials shown in (D). Data are presented as mean ± SEM and are representative of 3
1055 independent experiments. Statistical significance was assessed by one way ANOVA. (**F**)
1056 Western blot of indicated proteins were performed in THP1 cells transduced with lentivirus
1057 expressing either shCtrl, shCD84 (3'-UTR) or shCD84 (3'-UTR) plus CD84-WT. Data are
1058 representative of at least 2 independent biological replicates.

1059

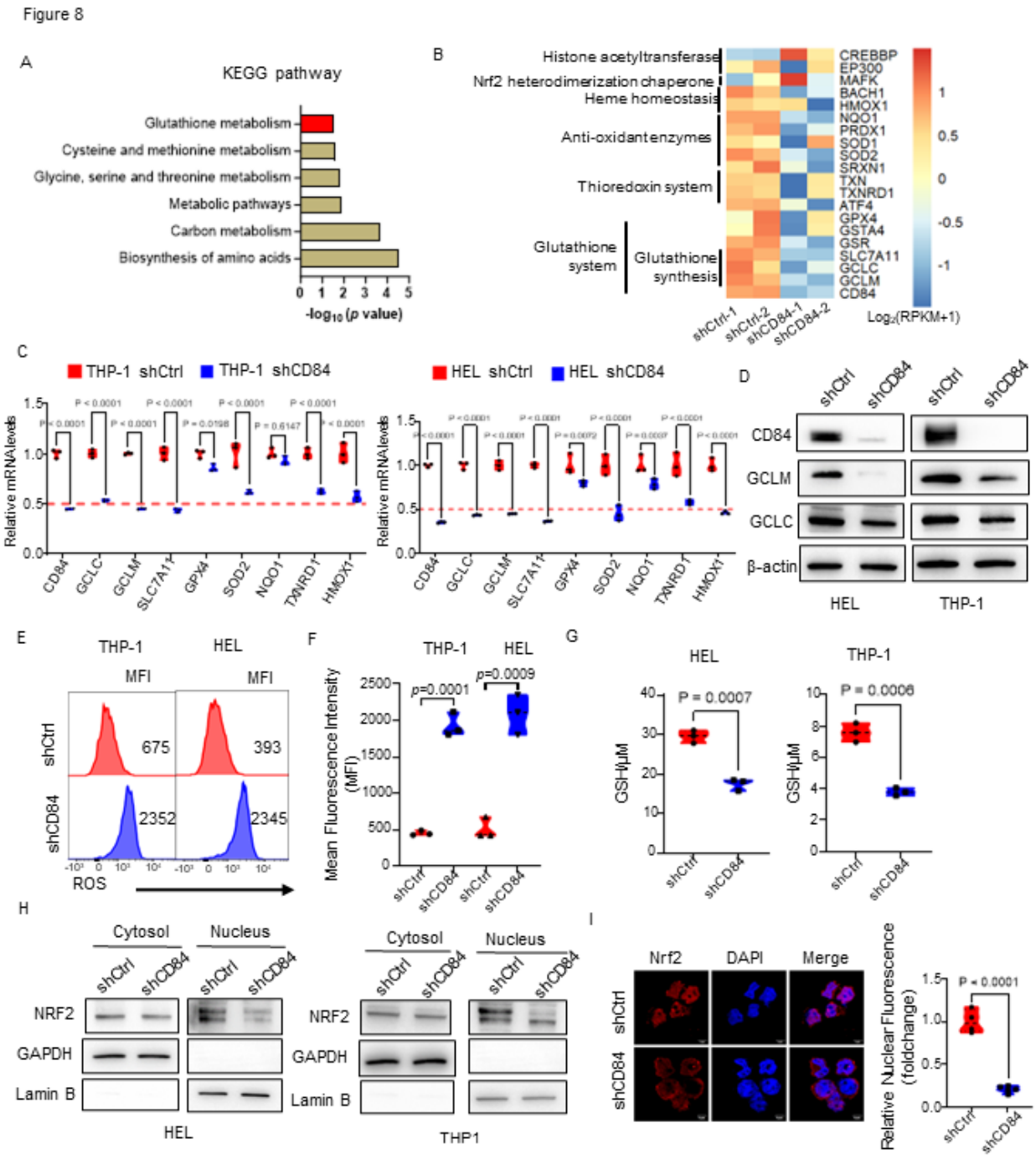

Figure 8. CD84 Knockdown Impairs Glutathione Metabolism and NRF2 Antioxidant Defense, Leading to Mitochondrial Dysfunction in AML. (**A**) Bar chart showing the KEGG pathway enrichment analysis of differentially expressed core genes in both THP1 cells and HEL cells. (**B**) Heatmap visualization of NRF2-regulated antioxidant and

1065 detoxification enzyme expression accorrding to our RNA-seq dataset. (**C**) The violin plot
1066 showing the mRNA expression of key anti-oxidant/detoxification genes THP1 cells and
1067 HEL cells transduced with shCtrl or shCD84. Data are presented as mean ± SEM and
1068 are representative of 3 independent experiments. Statistical significance was assessed
1069 by two tailed unpaired t test. (**D**) Immunoblot detection of indicated proteins involved in
1070 glutathione biosynthesis in THP1 cells and HEL cells transduced with shCtrl or shCD84
1071 for 72 hrs. Data are representative of at least 2 independent biological replicates. (**E-F**)
1072 Representative histogram (**E**) and violin chart (**F**) showing the effects of CD84 knockdown
1073 on intracellular ROS generation in THP1 cells and HEL cells transduced with shCtrl or
1074 shCD84 for 72 hrs. Data are presented as mean ± SEM and are representative of 3
1075 independent experiments. Statistical significance was assessed by two tailed unpaired t
1076 test. (**G**) The violin chart shows the intracellular GSH level in THP1 cells and HEL cells
1077 which were transduced with shCtrl or shCD84 for 72 hrs. Data are presented as mean ±
1078 SEM and are representative of 3 independent experiments. Statistical significance was
1079 assessed by two tailed unpaired t test. (**H**) Immunoblot analysis of the expression of
1080 NRF2 in the cytoplasm and nucleus of HEL and THP1 cells stably expressing CD84
1081 shRNA (targeting 3'UTR). Data are representative of at least 2 independent experiments.
1082 (**I**) Representative confocal microscopy images and violin chart showing the nucleoplasm
1083 distribution of NRF2 in THP1 cell transduced with either shCtrl or shCD84 lentivirus. The
1084 intensity of nuclear fluorescence were quantified in violin chart. Data are presented as
1085 mean ± SEM and are representative of 4 independent images. Statistical significance was
1086 assessed by two tailed unpaired t test.

1087

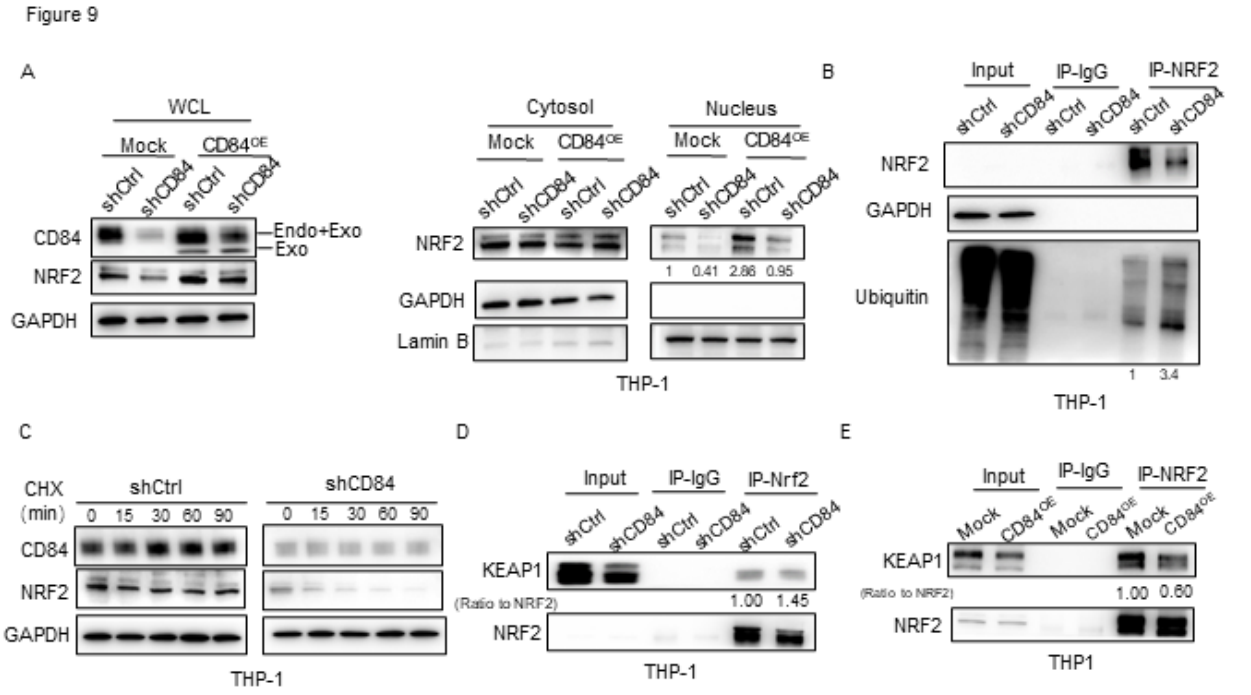

Figure 9. CD84 knockdown disrupts NRF2 binding to Keap1 in AML cells. (**A**) The immunoblot shows the expression of indicated proteins in THP1 cells transduced with shCtrl or shCD84. THP-1 cells stably expressing 3xFlag-CD84 were further infected with viruses expressing CD84 shRNA. The amount of NRF2 in the whole cell lysate, cytoplasm and nucleus was determined by immunoblot. (**B**) The immunoblot shows Co-IP analysis of the ubiquitination of NRF2 upon CD84 knockdown in THP1 cells. (**C**) The immunoblot shows the time course of protein expression after cyclohexamide (CHX) treatment with indicated time. Western blot analysis confirmed the presence of NRF2 at times after CHX treatment in control samples. (**D-E**) The immunoblot shows quantitative analysis of the binding to KEAP1 in the presence or absence of stably overexpressing Flag-CD84 cells by immunoprecipitation. The interaction between NRF2 and KEAP1 under different CD84 levels was analyzed. Indicated THP-1 cells stably expressing CD84 shRNA (**D**) or 3xFlag-

1101 CD84 (**E**) were harvested for immunoprecipitation and subjected to immunoblotting with
1102 anti-NRF2 and anti-KEAP1 antibodies. Data in A through E are representative of at least
1103 2 biological replicates.

1104

1105

1106

1107